Cell Reports

Article

Primate neuronal connections are sparse in cortex as compared to mouse

Graphical abstract

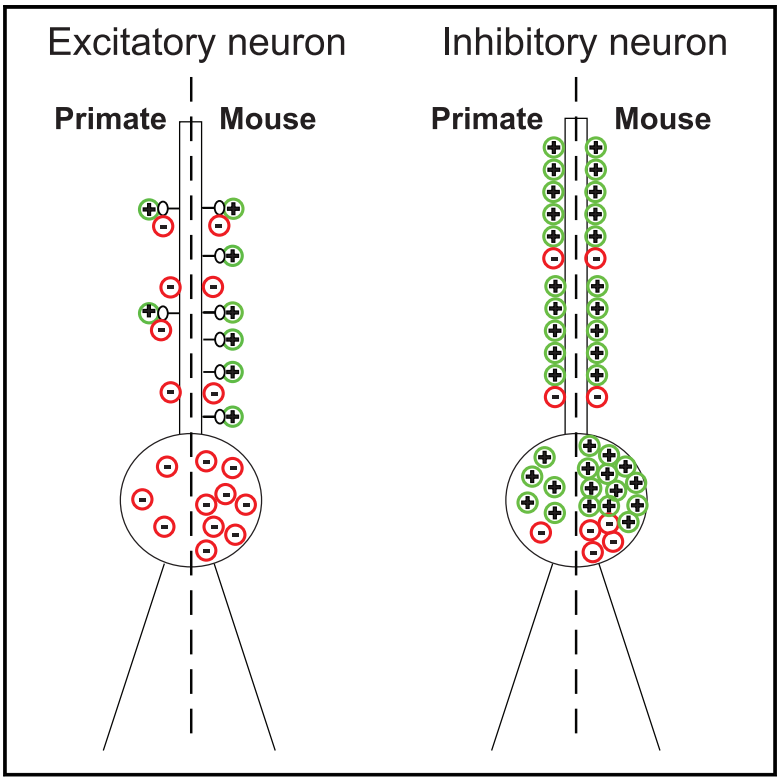

Highlights

- Relative to mouse counterparts, primate connections are sparse
- Primate excitatory neurons receive fewer excitatory and inhibitory inputs
- Primate inhibitory neurons have fewer somatic inputs but equivalent shaft inputs
- Across species, inhibitory axons have similar innervation properties

Authors

Gregg A. Wildenberg, Matt R. Rosen, Jack Lundell, Dawn Paukner, David J. Freedman, Narayanan Kasthuri

Correspondence

gwildenberg@uchicago.edu (G.A.W.), bobbykasthuri@uchicago.edu (N.K.)

In brief

Using large-volume serial electron microscopy, Wildenberg et al. show that primate cortical neural networks are sparser than mouse, and using recursive neural nets, they show that energetic costs of synaptic maintenance could underlie these differences.

Wildenberg et al., 2021, Cell Reports *36*, 109709
September 14, 2021
https://doi.org/10.1016/j.celrep.2021.109709

CellPress

Cell Reports

CellPress
OPEN ACCESS

Article

Primate neuronal connections are sparse in cortex as compared to mouse

Gregg A. Wildenberg,[1,2,*] Matt R. Rosen,[1] Jack Lundell,[1] Dawn Paukner,[1] David J. Freedman,[1] and Narayanan Kasthuri[1,2,3,*]

[1]Department of Neurobiology, University of Chicago, Chicago, IL 60637, USA
[2]Argonne National Laboratory, Lemont, IL 60439, USA
[3]Lead contact
*Correspondence: gwildenberg@uchicago.edu (G.A.W.), bobbykasthuri@uchicago.edu (N.K.)
https://doi.org/10.1016/j.celrep.2021.109709

SUMMARY

Detailing how primate and mouse neurons differ is critical for creating generalized models of how neurons process information. We reconstruct 15,748 synapses in adult Rhesus macaques and mice and ask how connectivity differs on identified cell types in layer 2/3 of primary visual cortex. Primate excitatory and inhibitory neurons receive 2–5 times fewer excitatory and inhibitory synapses than similar mouse neurons. Primate excitatory neurons have lower excitatory-to-inhibitory (E/I) ratios than mouse but similar E/I ratios in inhibitory neurons. In both species, properties of inhibitory axons such as synapse size and frequency are unchanged, and inhibitory innervation of excitatory neurons is local and specific. Using artificial recurrent neural networks (RNNs) optimized for different cognitive tasks, we find that penalizing networks for creating and maintaining synapses, as opposed to neuronal firing, reduces the number of connections per node as the number of nodes increases, similar to primate neurons compared with mice.

INTRODUCTION

The primary visual systems of *Mus musculus* and *Macaca mulatta* are the two dominant models for understanding cortical processing at the level of individual neurons, with expansive literatures on morphological, functional, and molecular properties of different neuronal classes (Bakken et al., 2016; Bernard et al., 2012; Gilman et al., 2017; Gouwens et al., 2018, 2019; Gur and Snodderly, 2008; Medalla and Luebke, 2015; Ohki et al., 2005; Tasic et al., 2016, 2018). Comparisons across both would allow a better understanding of how neuronal cell types change their connectivity across brains of such disparate size and neuronal number (Herculano-Houzel, 2009, 2011) and whether these changes affect properties of neuronal networks, including excitatory-to-inhibitory (E/I) balances (Brunel, 2000; Isaacson and Scanziani, 2011; Kremkow et al., 2010; van Vreeswijk and Sompolinsky, 1996; Vogels and Abbott, 2009) and inter-neuronal connectivity. Although molecular and functional comparisons continue (Bakken et al., 2020; Hodge et al., 2019; Krienen et al., 2020; Wang et al., 2016), large-scale connectivity comparisons across primate and mouse brains are often limited to comparisons of synaptic density in neuropil, without reference to neuronal type, synapse location, or relative changes in types of synapses on single neurons. Furthermore, as much of the prior literature focuses on optical reconstructions of synaptic proxies such as spines, data on inhibitory connectivity remain scarce, as such connectivity cannot be easily inferred from light-level reconstructions.

We applied recent advances in large-volume, automated serial electron microscopy (EM) (i.e., "connectomics") (Baena et al., 2019; Briggman et al., 2011; Gour et al., 2021; Hayworth et al., 2020; Januszewski et al., 2018; Turner et al., 2020; Vishwanathan et al., 2020; Yin et al., 2020) to compare connectivity of excitatory and inhibitory neurons in layer 2/3 (L2/3) of primary visual cortex (V1) of mouse (*Mus musculus*) and primate (*Macaca mulatta*). We looked on excitatory and inhibitory neurons across species for differences in innervation densities of different classes of synapses (i.e., spine, shaft, and soma) and therefore changes in proportions between (i.e., E/I ratios) and changes in how individual neurons were wired together.

RESULTS

We reconstructed neurons and their connections using a multiscale EM-based connectomics approach targeting L2/3 in "adult" V1 from three mice (one dataset generated and two publicly available; Bock et al., 2011; Lee et al., 2016) and two primates (male, 11 and 14.5 years of age; see STAR Methods). We chose time points past a majority of brain developmental milestones and before the onset of age-associated pathologies for both species (Bakken et al., 2016; Bourgeois and Rakic, 1993; Horton and Hocking, 1997; Lee et al., 2000; Peters et al., 1996; Scott et al., 2016; Semple et al., 2013). We chose L2/3 for several reasons. First, dendritic arbors of neurons in both species are comparable in size (Gilman et al., 2017), so comparisons of connectivity could be "normalized" to neuronal size. Second, L2/3 neurons in both species have smaller dendritic arbors (Rojo et al., 2016) (e.g., compared with dendritic arbors of layer 5 neurons), allowing analyses in limited-volume EM datasets of a larger fraction of all the synapses on a particular neuron. Third, there seems to be a limited number of morphological cell

types in L2/3 (Gouwens et al., 2019; Radnikow and Feldmeyer, 2018; Wang et al., 2018), increasing the probability that our measurements reflect comparisons among similar cell types.

We prepared 300-μm-thick coronal sections spanning V1 as previously described (Hua et al., 2015) and collected 3,000 ultra-thin sections using the ATUM (automated tape-collecting ultramicrotome) approach (Kasthuri et al., 2015) from mouse (each section 0.8 mm × 1.5 mm × 40 nm) and primate (0.8 mm × 2.4 mm × 40 nm), where each individual section spanned all cortical layers in both species (Figures S1A and S1B). We imaged all cortical layers using low-resolution EM (~40 nm in-plane resolution) and skeletonized the dendritic arbors contained within the imaged volume of 102 primate neurons and 68 mouse neurons across all cortical layers (Figures S1A and S1B; V1 40 nm imaged volumes: primate, 0.8 × 2.4 × 0.07 mm; mouse, 0.8 × 1.5 × 0.07 mm). We used these low-resolution reconstructions to identify and measure L2/3 neuronal shapes and densities between species and for subsequent synaptic level reconstructions.

Consistent with previous reports, we found little differences in the cytoarchitecture or morphology of L2/3 neurons across species. For both primate and mouse, excitatory somata were distributed at similar densities when measured both as the distance between every soma (Figure S1C) and soma/mm^3 (primate, 2.3e5 ± 1.7e4, n = 2 primates; mouse, 2.7e5 ± 2.1e4, n = 3 mice; p = 0.3, Mann-Whitney test). Similarly, primate and mouse excitatory neurons had a similar number of dendritic branchpoints per neuron (Figure S1D) and similar somatic surface areas (Figure S1E), and the total length of dendrite per neuron was slightly larger in mouse (Figure S1F), again consistent with prior findings (Gilman et al., 2017).

We next reimaged a smaller volume surrounding L2/3 at high resolution in both species (~6 nm in-plane resolution: mouse, 100 × 100 × 30 μm; primate, 100 × 90 × 30 μm and 115 × 115 × 30 μm) and used two publicly available mouse L2/3 V1 connectomes (public mouse data: 80 × 80 × 30 μm at ~4 nm in-plane resolution for both). We annotated 9,764 synapses and 711 axons that synapsed onto 72 excitatory and 9 inhibitory neurons in the three mouse samples and 5,984 synapses and 372 axons that synapsed on 91 excitatory and 16 inhibitory neurons across two primates (see Figures S1G and S1H for example reconstructions and total volume imaged, and see Videos S1 and S2 as examples of our data quality). Visual inspection of the neurons (Figure S2) revealed that the majority in both species were pyramidal with apical pointing dendrites and that 3 of 37 somata in the mouse and 9 of 42 primate somata were inhibitory neurons, agreeing with previously reported proportions of pyramidal neurons (Gouwens et al., 2019; Kanari et al., 2019) and ratios of excitatory and inhibitory neurons (Džaja et al., 2014; Sultan and Shi, 2018). We next analyzed the connectivity of different neuronal compartments (e.g., dendrites, soma) across species, classifying each synapse as a spine, shaft, somatic, or perisomatic synapse on the basis of a prior schema (Freund and Katona, 2007) and each axon as excitatory or inhibitory on the basis of whether they predominantly innervated spines or shafts and somata, respectively (Harris and Weinberg, 2012).

For dendrites, we counted spine and shaft synapses at different dendritic locations relative to the soma to account for synapse variability within a neuron's dendritic tree. (Ballesteros-Yáñez et al., 2006; Benavides-Piccione et al., 2013; Vaudin et al., 1988). We also sampled random dendrites with different diameters and orientations to ensure that our results were not biased toward proximal dendrites, making sure to include in our analysis the thinnest possible dendrites that are likely to be the most distal (Stuart et al., 2016). Because the vast majority of excitatory neurons were pyramidal in both species, we excluded the rare non-pyramidal excitatory neurons from our analyses. We compiled all metrics described below in Table 1, with individual values for each measurement listed (mean, SEM, sample size, and p value).

Somatic and dendritic innervation of excitatory primate and mouse neurons

Primate L2/3 excitatory neurons had large differences in the numbers of specific types of synapses received relative to the mouse. Figure 1A shows a representative example of a reconstructed primate and mouse excitatory neuron. The example primate excitatory neuron had ~5-fold lower dendritic spine synapses relative to the mouse, throughout the dendritic arbor (Figure 1A, dendrite insets: primate, 0.24 excitatory spine synapses/μm; mouse, 1.15 excitatory spine synapses/μm). Similarly, the example primate soma received 20 somatic and perisomatic synapses (henceforth collectively called "somatic synapses"), while the example mouse soma received 66 somatic synapses (Figure 1A, soma inset). The frequency of shaft synapses (i.e., synapses directly on dendrites) was lower than that of spine synapses in both species, with similar densities across species (0.18 shaft synapses/μm for primate, 0.12 shaft synapses/μm for mouse), unlike spine or somatic synapses. We found consistent results across multiple neurons and multiple primate and mouse samples (n = 26 excitatory neurons across two mice and two primates; see Table 1). For all dendritic synapse measurements, quantifications from apical and basal dendrites were pooled, as we found little difference across apical and basal spine or shaft synapse densities in either species (data not shown). Compared with similar mouse excitatory neurons, primate neurons received ~2.5-fold fewer spine synapses (Figure 1B) and 4-fold fewer somatic synapses (Figure 1C) but equivalent rates of shaft synapses (Figure 1D). Both primate and mouse excitatory neurons showed a similar trend in spine density along dendrites: spine synapses were completely absent in the perisomatic region, consistent with prior reports (Emoto et al., 2016; Megías et al., 2001), and spine density increased as a function of distance from the soma (Figure 1B). The furthest distance of dendrite examined in both species was 148 μm from the soma in mouse and 115 μm in the primate (but see below).

Although primate excitatory neurons receive 3-fold fewer spine synapses, individual spines of primate neurons were 3-fold more likely to receive a second, inhibitory synapse (Jones and Powell, 1969; Knott et al., 2002; Kwon et al., 2019) (Figure 1E). Using these averages and mean dendritic arbor lengths for primate and mouse L2/3 neurons as previously reported (Gilman et al., 2017), we calculated the ratio of the total number of excitatory and inhibitory inputs onto individual excitatory neurons (see STAR Methods): mouse excitatory neurons received 6,894 total connections (5,847 excitatory and 1,048 inhibitory),

Table 1. Summary table listing quantifications from this report

	Mouse V1	Primate V1	Number of biological features	Number of animals	p value	Fold change in primate
Measurement (mean ± SEM)						
Excitatory neurons						
Soma density (μm)	53.3 ± 0.4	47.6 ± 0.3	ms: 62 neurons; pr: 71 neurons	ms: 1; pr: 1	2.8e-3	1.11× lower
Soma surface area (μm^2)	370 ± 12.4	387 ± 20.8	ms: 6 neurons; pr: 8 neurons	ms: 1; pr: 1	0.3	n.c.
Branch number/neuron	18.0 ± 0.9	16.2 ± 1.2	ms: 20 neurons; pr: 47 neurons	ms: 1; pr: 1	0.08	n.c.
Total dendritic length (μm)	683 ± 46	399 ± 41	ms: 20 neurons; pr: 47 neurons	ms: 1; pr: 1	1e-5	1.7× lower
Spine synapses/μm	2.34 ± 0.1	1.1 ± 0.03	ms: 82 10 μm dendrite fragments on 10 neurons; pr: 175 10 μm dendrite fragments on 16 neurons	ms: 1; pr: 2	3.6e-5	2.1× lower
**Spine synapses/μm	1.34 ± 0.1	0.56 ± 0.03	ms: 82 10 μm dendrite fragments on 10 neurons; pr: 175 10 μm dendrite fragments on 16 neurons	ms: 1; pr: 2	1.5e-14	2.4× lower
Shaft synapses/μm	0.18 ± 0.02	0.19 ± 0.01	ms: 82 10 μm dendrite fragments on 10 neurons; pr: 175 10 μm dendrite fragments on 16 neurons	ms: 1; pr: 2	0.23	n.c.
Synapses/(peri)soma	95.8 ± 3.9	24.8 ± 1.9	ms: 1,341 synapses on 14 neurons; pr: 323 synapses on 13 neurons	ms: 3; pr: 2	1.0e-7	3.9× lower
Second spine synapses (%)	3.0 ± 0.0	11.0 ± 0.0	ms 180 spines on 3 neurons; pr: 437 spines on 7 neurons	ms: 1; pr: 2	6.6e-4	3.7× higher
Estimated total excitatory synapses	5,846 ± 626	1,790 ± 281	ms: 770 spines on 4 neurons; pr: 669 spines on 7 neurons	ms: 1; pr: 1	6.0e-3	3.3× lower
Estimated total inhibitory synapses	1,048 ± 22	759 ± 59	ms: 109 shaft, 401 soma synapses on 4 neurons; pr: 207 shaft, 173 soma synapses on 7 neurons	ms: 1; pr: 1	6.0e-3	1.4× lower
E/I	5.55 ± 0.5	2.42 ± 0.4	(combined total of estimated total excitatory and estimated total inhibitory synapses)	ms: 1; pr: 1	6.1e-3	2.3× lower
Inhibitory neurons						
Shaft synapses/μm	2.3 ± 0.5	1.1 ± 0.4	ms: 39 10 μm dendrite fragments on 4 neurons; pr: 58 10 μm dendrite fragments on 10 neurons	ms: 1; pr: 2	0.32	n.c.
**Shaft synapses/μm	2.7 ± 0.1	1.7 ± 0.1	ms: 39 10 μm dendrite fragments on 4 neurons; pr: 58 10 μm dendrite fragments on 10 neurons	ms: 1; pr: 2	3.3e-8	1.6× lower
Synapses/(peri)soma	207 ± 18	44 ± 7	ms: 1,653 synapses on 8 neurons; pr: 307 synapses on 7 neurons	ms: 3; pr: 2	3.1e-4	4.7× lower
E/I	4.93 ± 0.9	5.3 ± 1.2	ms: 226 axons across 7 dendrites, 242 axons across 4 soma; pr: 202 axons across 7 dendrites, 109 axons across 3 soma	ms: 2; pr: 2	1.0	n.c.

(*Continued on next page*)

Table 1. *Continued*

	Mouse V1	Primate V1	Number of biological features	Number of animals	p value	Fold change in primate
Somatic innervating axons						
*Branches/μm	1.4 ± 0.3	1.4 ± 0.5	ms: 57 axons; pr: 39 axons	ms: 1; pr: 1	0.7	n.c.
*Bouton surface area (μm)	1.9 ± 0.1	1.9 ± 0.1	ms: 84 boutons on 2 neurons; pr: 44 boutons on 2 neurons	ms: 1; pr: 1	0.7	n.c.
*Synapses/μm	0.22 ± 0.0	0.27 ± 0.0	ms: 1,118 synapses on 57 axons; pr: 857 synapses on 39 axons	ms: 1; pr: 1	4.9e-4	1.1× higher
*Peri(soma) synapses/axon	2.3 ± 0.1	1.3 ± 0.2	ms: 381 synapses on 163 axons; pr: 115 synapses on 60 axons	ms: 1; pr: 1	0.07	n.c.
Axons/soma	38 ± 3	14 ± 1	ms: 198 axons on 5 soma; pr: 84 axons on 6 soma	ms: 1; pr: 1	2.1e-3	2.7× lower
% shared (nearest neighbor)	21 ± 0.0	40 ± 0.0	ms: 188 axons, 504 synapses on 3 neuron pairs; pr: 60 axons, 162 synapses on 3 neuron pairs	ms: 1; pr: 1	0.1	n.c.

SEM and p values for each measurement except those noted with an asterisk were calculated with sample size (n) being the number of neurons. SEM and p value for datasets marked with a double or single asterisk were derived using the sample size as the number of 10 μm dendrite fragments or axons, respectively. Measurements between mouse and primate for which $p > 0.05$ are marked as no change (n.c.).

and primate excitatory neurons received on average 2,558 total connections (1,806 excitatory and 753 inhibitory). Thus, the average E/I ratio in primate excitatory neurons was 2.3-fold lower than the average E/I ratio in mice (Figure 1F).

Somatic and dendritic innervation of inhibitory primate and mouse neurons

We saw a similar trend of reduced synapse numbers onto primate inhibitory neurons. In the same volume (Figure S2), we identified inhibitory neurons on the basis of the relative sparsity of spines on their dendrites (Freund and Buzsáki, 1996; Gulyás et al., 1999; see bottom panel, Figure S2). In example neurons shown in Figure 2A, we found that the primate inhibitory neuron received ~1.5-fold fewer shaft synapses than the mouse inhibitory neuron and 4-fold fewer somatic synapses (Figure 2A, dendrite and somatic insets: primate inhibitory neuron, 2.06 shaft synapses/μm and 39 somatic synapses compared with 3.00 shaft synapses/μm and 162 somatic synapses in the mouse). Across dendritic fragments compiled from many neurons, primate inhibitory neurons have a reduced shaft synapse/μm density when quantified across dendrite fragments (Figure 2B). However, when quantified across individual neurons, there is no statistical difference, suggesting a high degree of variability in shaft synapse density across individual neurons within each species (see Table 1). Across all neurons analyzed, however, primate inhibitory neurons consistently receive statistically fewer somatic synapses relative to mouse inhibitory neurons (Figure 2C).

Inhibitory neurons can receive both excitatory and inhibitory synapses throughout their dendritic shaft and soma (Emoto et al., 2016; Gulyás et al., 1999). However, unlike excitatory neurons in cortex, where synapses can be classified as excitatory or inhibitory on the basis of whether they synapse onto spines or shafts and soma, respectively (Harris and Weinberg, 2012; Hering and Sheng, 2001), classifying synapses as excitatory or inhibitory on dendrites of inhibitory neurons is difficult, as they are often aspinous (Ascoli et al., 2008; Goldberg et al., 2003; Gulyás et al., 1999). We instead calculated E/I ratios on individual neurons by identifying the innervating presynaptic axon as excitatory or inhibitory, leveraging Dale's law (Strata and Harvey, 1999). Specifically, for presynaptic axons innervating a specific interneuron, we identified other synapses they made in the volume as spine, dendritic shaft, soma, and so on, and identified their postsynaptic targets as excitatory or inhibitory neurons on the basis of the classification described above. Axons that made predominantly spine synapses on excitatory targets were labeled excitatory, and axons that made predominantly shaft and somatic synapses on excitatory neurons were labeled inhibitory (Figure S3). Figure 2D shows an example reconstruction used for this classification. Blue and green axons innervating the soma and dendrite (shown in red) were determined to be excitatory or inhibitory, respectively, by the above classification scheme. The insets show zoomed-in regions where axons synapsed with the target inhibitory neuron dendrite and soma and depict other annotated synapses (yellow spheres) used to classify each axon.

In the examples shown in Figure 2A, the primate inhibitory neuron had 3.8-fold greater innervation by excitatory neurons than inhibitory neurons, and a somatic E/I ratio of 2.6, while the mouse neuron dendritic and somatic E/I ratios were 9.6 and 1.7, respectively. However, unlike excitatory neurons, for which E/I balances across individual primate neurons were consistently lower than across mouse neurons, E/I balances of individual inhibitory neurons in both species varied widely (Figure 2E). This was due primarily to larger differences in the numbers of E and I inputs on soma, and as a result there was little statistical difference in inhibitory neuron E/I balances across species. Finally, we detailed the complete linear sequence of excitatory and inhibitory axons along each inhibitory dendrite analyzed,

CellPress
OPEN ACCESS

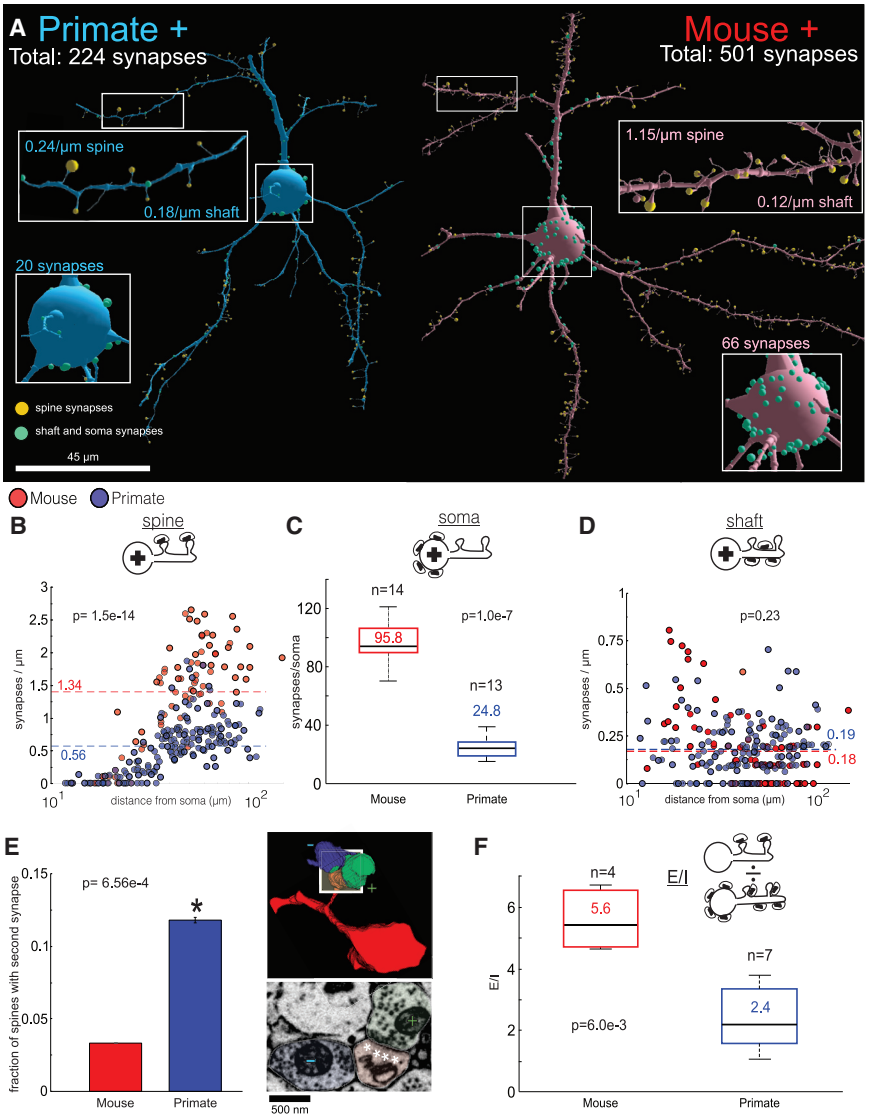

Figure 1. Mouse L2/3 excitatory neurons receive more connections than primate neurons

(A) EM reconstructions of morphologically matched L2/3 primate and mouse excitatory (+) neurons. Spine synapses are yellow spheres; dendritic shaft and somatic synapses are green spheres. Square inset: magnified views of soma: primate +, 20 total somatic synapses; mouse +, 66 total somatic synapses. Rectangle inset: magnified views of dendrites: primate +, 0.24 spine synapses/μm, 0.18 shaft synapses/μm; mouse +, 1.15 spine synapses/μm, 0.12 shaft synapses/μm.

(B) Scatterplot of excitatory neuron spine synapses/μm versus distance from soma (μm) (primate: 0.56 ± 0.03 synapses/μm, n = 175, 10 μm dendrite fragments across 16 neurons, two primates; mouse: 1.34 ± 0.09 synapses/μm, n = 82 10 μm dendrite fragments across 10 neurons, one mouse; p = 1.5e-14).

(C) Box-and-whisker plot of excitatory neuron total synapses/soma (mouse: 95.8 ± 3.9, n = 1,341 synapses across 14 soma, three mice; primate: 24.8 ± 1.9, n = 323 synapses across 13 soma, two primates; p = 1.0e-7).

(D) Scatterplot of excitatory neuron shaft synapses/μm versus distance from soma (μm) in excitatory neurons (primate: 0.19 ± 0.01 synapses/μm, n = 175, 10 μm dendrite fragments counted across 16 neurons, two primates; mouse: 0.18 ± 0.01 synapses/μm, n = 82, 10 μm dendrite fragments counted across 10 neurons, one mouse; p = 0.23).

(E) Bar plot of the fraction of spines with second synapses (primate: 0.11 ± 0.001, n = 437 spines across 7 neurons, two primates; mouse: 0.03 ± 0.00, n = 180 spines across 3 neurons, one mouse; p = 6.56e-4). Right inset: three-dimensional (3D) reconstruction (top) and matched 2D EM (bottom) image of a primate dendritic spine (red) with a second synapse: an excitatory synapse on the spine head (green/+) and inhibitory synapse on the side (blue/−). Asterisks show the postsynaptic density.

(F) Box-and-whisker plot of the excitatory-to-inhibitory synapse (E/I) ratio on excitatory neurons (see STAR Methods) (mouse: 5.55 ± 0.48, n = 770 spine synapses [180 scored for second spine synapses], 109 shaft synapses, and 401 somatic/perisomatic synapses over 4 neurons; primate: 2.04 ± 0.4, n = 669 spine synapses [377 scored for second spine synapses], 207 shaft synapses,173 somatic/perisomatic synapses over 7 neurons, two primates; p = 6.0e-3). All quantifications represent mean ± SEM; p values were calculated using a two-tailed Mann Whitney U test with a 0.05 significance level.

and in both species, we saw long stretches of excitatory synapses interspersed with inhibitory connections (Figure 2D, top; Figure S4).

Sparse connectivity as a general phenomenon of primate cortex

We tested two alternative explanations: (1) differences in spine and synapse density are limited to only proximal dendrites, because the limited EM volumes imaged do not contain entire dendritic arbors, and (2) synapse differences are specific to V1. We focused on the most significant differences reported above: excitatory spine synapse density and excitatory and inhibitory soma synapse number. In three mice and two primate V1 datasets, we first randomly selected excitatory dendrites and reconstructed all spine synapses on them (n = 100 10 μm dendrite fragments sampled across three mouse datasets [~30 dendrites in each dataset] and n = 101 10 μm dendrite fragments across two primate datasets [~50 dendrites in each dataset]; results summarized in Table S1). The sampled dendritic fragments ranged in orientation and diameter in both species (Figures 3A and S5), suggesting that many, particularly those with the smallest diameters, were likely from distal parts of dendritic arbors (Bannister and Larkman, 1995; Stuart et al., 2016). Among this population, we saw clear decreases in spine synapse density in primates relative to the mouse, independent of diameter (Figure 3B) or orientation (data not shown). These decreases were similar in magnitude as observed from more proximate parts of mouse and primate dendrites (Figure 1).

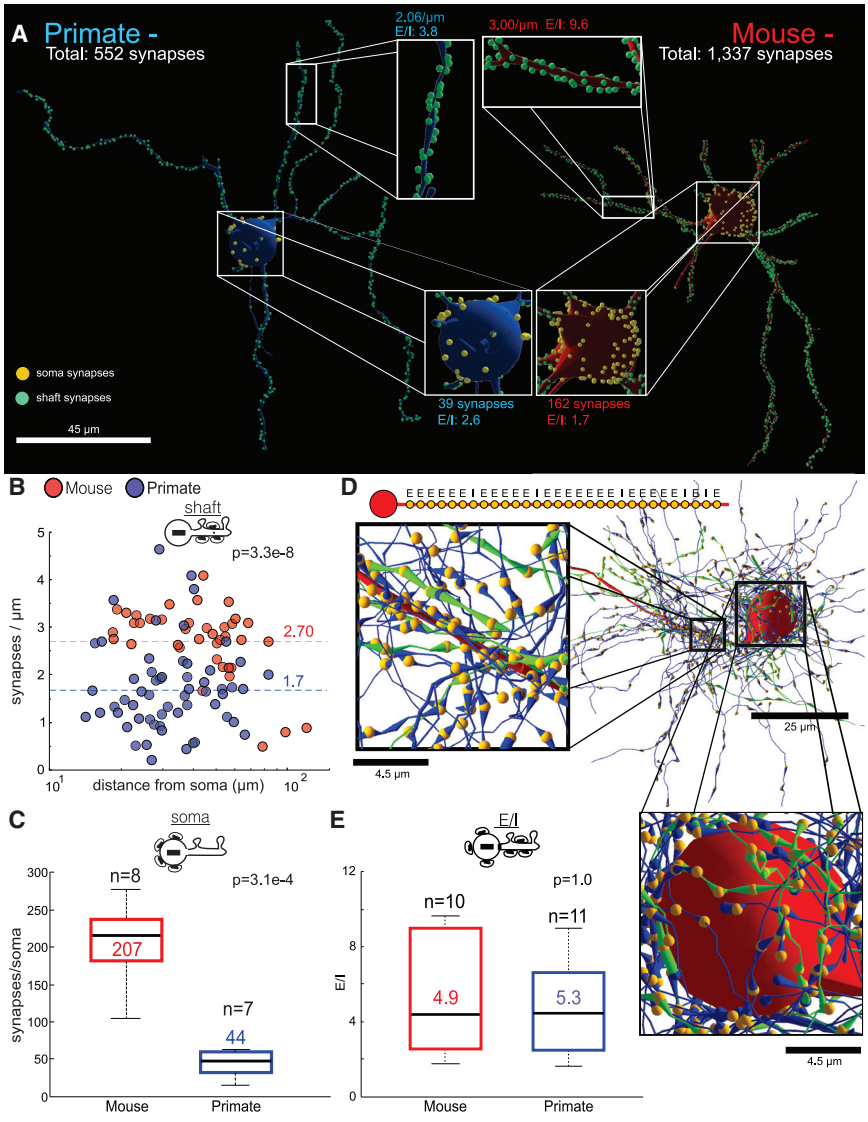

Figure 2. Mouse L2/3 inhibitory neurons receive more connections than primate neurons

(A) Representative EM reconstructions of morphologically matched L2/3 primate and mouse inhibitory (–) neurons. Soma synapses are orange spheres; dendritic shaft synapses are green spheres. Square inset: magnified views of soma: primate –, 39 total somatic synapses, somatic E/I = 2.6; mouse –, 162 total somatic synapses, somatic E/I = 1.7. Rectangle inset: magnified views of dendrites: primate (–), 2.06/µm shaft synapses/µm, dendritic E/I = 3.8; mouse (–), 3.00 shaft synapses/µm, dendritic E/I = 9.6.

(B) Scatterplot of inhibitory neuron shaft synapses/µm versus distance from soma (µm) (primate: 1.7 ± 0.1 synapses/µm, n = 58, 10 µm dendritic fragments across 10 neurons, two primates; mouse: 2.70 ± 0.12 synapse/µm, n = 39 10 µm dendrite fragments across 4 neurons, one mouse; p = 3.31e-8).

(C) Box-and-whisker plot of inhibitory neuron synapses/soma (mouse: 207 ± 18, n = 1,653 synapses across 8 soma, three mice; primate: 44 ± 6.6, n = 307 synapses across 7 soma, two primates; p = 3.1e-4).

(D) Reconstruction of the soma and a single dendrite of mouse inhibitory neuron (red). Radiating off the soma and dendrite are excitatory (blue) and inhibitory (green) axons that make shaft synapses on that dendrite. Left: zoom-in showing region where excitatory (blue) and inhibitory (green) axons make synapses with the inhibitory neuron dendrite. Bottom right: zoom-in showing the soma with all excitatory (blue) and inhibitory (green) axons that make synapses on the soma. All synapses onto neighboring neurons (not depicted) were marked and annotated as orange spheres. Top: cartoon of mouse inhibitory neuron and single dendrite showing the continuous sequence of excitatory (E) and inhibitory (I) synapses made along the dendrite.

(E) Box-and-whisker plot of the combined dendritic and somatic excitatory to inhibitory (E/I) ratio of inhibitory neurons (mouse: 4.93 ± 0.9, n = 226 axons scored across 7 dendrites, 242 axons across 4 soma, two mice; primate: 5.28 ± 1.2, n = 202 axons across 7 dendrites, 109 axons across 3 soma, two primates; p = 1.0.

All quantifications represent mean ± SEM; p values were calculated using a two-tailed Mann Whitney U test with a 0.05 significance level.

To address the possibility that reduced synapse density is peculiar to primate V1, in the same primate brains we collected V1 datasets from, we randomly sampled 110 10 µm dendrite fragments and reconstructed four soma and somatic synapses in primary somatosensory cortex (S1) and 72 10 µm dendrite fragments and 11 soma and somatic synapses in the lateral intraparietal cortex (LIP), a higher order mixed sensory and motor cortical region (Huk et al., 2017) (Figure 3C; see STAR Methods). We find, like primate V1, that spine synapses are ~3.4-fold reduced in S1 and LIP primate excitatory neurons relative to mouse V1 (Figure 3D). Furthermore, excitatory and inhibitory neurons received ~3.5-fold fewer somatic synapses relative to mouse V1 (Figures 3E and 3F). We conclude that sparsity in the primate brain likely extends to other brain regions and beyond proximal dendrites.

Inhibitory innervation patterns onto primate and mouse excitatory neurons

We next asked how changes in numbers of connections on individual neurons correlated with how neurons connect with one another. We focused on reconstructing the innervation patterns of axons synapsing with the soma of excitatory neurons, as we could reasonably assume that these axons primarily come from parvalbumin (PV+) inhibitory neurons that preferentially target soma and the most proximal portion of dendrites (Goldberg and Yuste, 2005; Karube et al., 2004; Kawaguchi and Kubota, 1997; Kisvárday et al., 1985; Somogyi, 1989; Tremblay et al., 2016), and thus we expected to be able to capture a majority of the connections these axons make to neuronal targets within our imaged volume. We first characterized basic properties of these somatic targeting inhibitory axons across species (e.g., axonal branching,

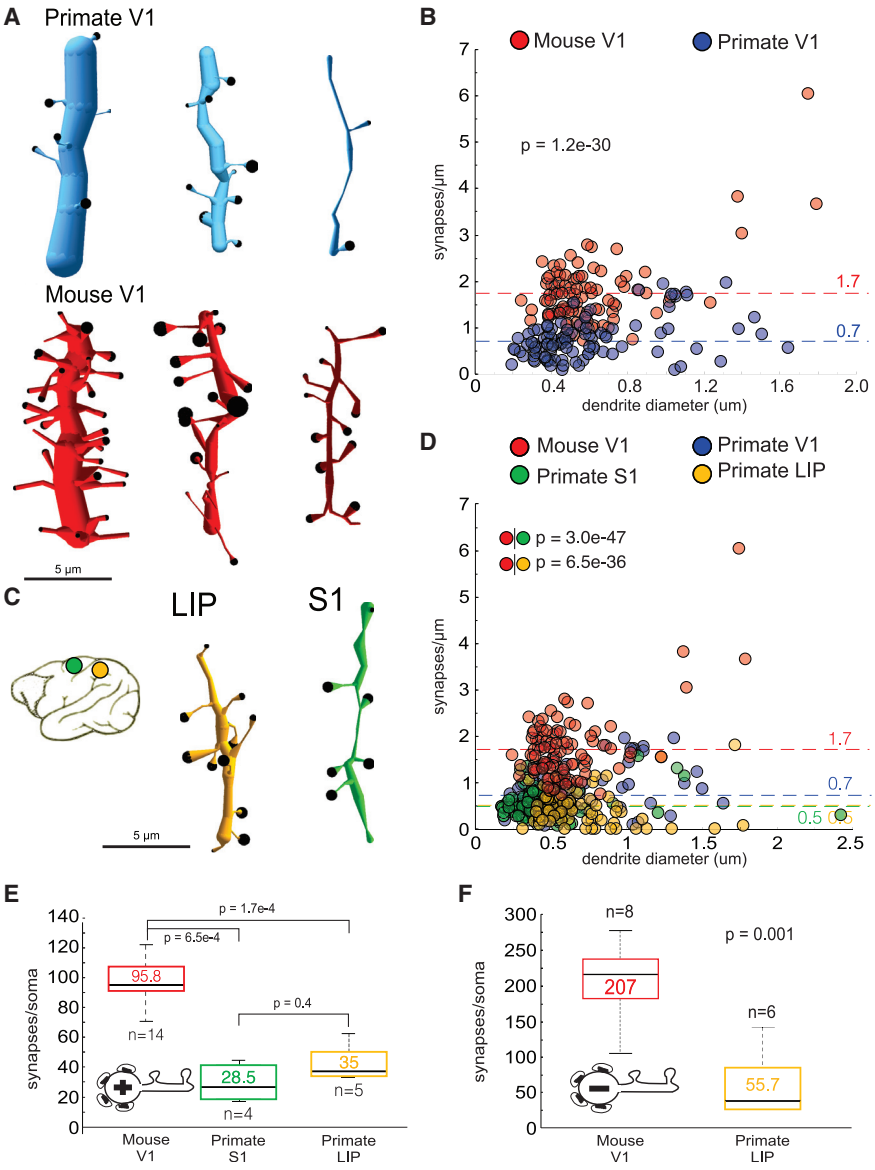

Figure 3. Reduced connectivity in primate compared with mouse is general across individuals and cortical areas

(A) Reconstructions of representative randomly sampled dendrites from primate (blue) and mouse (red). Reconstructions depict the approximate diameter of each dendrite and represent the classes of largest, medium, and smallest dendrites sampled.

(B) Scatterplot of excitatory neuron spine synapses/µm versus dendrite diameter (µm) (mouse V1: 1.7 ± 0.07 synapses/µm, n = 100, 10 µm dendrite fragments, three mice; primate V1: 0.7 ± 0.04 synapses/µm, n = 101 dendrite fragments, two primates; p = 1.2e-30).

(C) Left: cartoon of additional primate brains regions used to compare with V1; right: representative reconstructions of randomly sampled dendrites from the two brain regions (yellow, LIP; green, S1).

(D) Scatterplot of excitatory neuron spine synapses/µm versus dendrite diameter (µm) (mouse V1: 1.7 ± 0.07 synapses/µm, n = 100, 10 µm dendrite fragments, three mice; primate V1: 0.7 ± 0.04 synapses/µm, n = 101 dendrite fragments, two primates; primate S1: 0.5 ± 0.03 synapses/µm, n = 110, 10 µm dendrite fragments, two primates; primate LIP: 0.5 ± 0.05 synapses/µm, n = 72, 10 µm dendrite fragments, one primate; mouse V1 versus primate S1, p = 3.0e-47; mouse V1 versus primate LIP: 6.5e-36).

(E) Box-and-whisker plot of total excitatory neuron synapses/soma (mouse V1: 95.8 ± 3.8, n = 1,341 synapses across 14 soma, three mice; primate S1: 28.5 ± 5.9, n = 114 synapses across 4 soma, one primate; primate LIP: 35 ± 5.3, n = 175 synapses across 5 soma, one primate; mouse V1 versus primate S1, p = 6.5e-4; mouse V1 versus primate LIP, p = 1.7e-4; primate S1 versus primate LIP, p = 0.4).

(F) Box-and-whisker plot of inhibitory neuron synapses/soma (mouse V1: 207 ± 18.3, n = 1,653 synapses across 8 soma, three mice; primate LIP: 55.7 ± 18.3, n = 334 synapses across 6 soma, one primate; p = 0.001).

All quantifications represent mean ± SEM; p values were calculated using a two-tailed Mann Whitney U test with a 0.05 significance level.

bouton size, and synapse frequency along axons) and found that despite large differences in the absolute numbers of somatic connections, these basic properties were similar across mouse and primate inhibitory axons. Inhibitory axons in primate branched similarly to mouse (Figure S6A) and made synapses as frequently (Figure S6B). Furthermore, reconstructions of axons innervating the soma of mouse and primate excitatory neurons revealed that somatic innervating axons in the mouse made on average 2.34 ± 0.1 synapses on each soma, slightly more frequent than the primate (1.33 ± 0.15) (Figure S6C). Thus, the ~4-fold increase in somatic synapse number on mouse excitatory neurons was primarily the result of more axons innervating each soma (Figure S6D). Finally, the absolute difference in somatic synapse number on individual neurons was accompanied by little change in the size of inhibitory synapses (Figure S6E).

One possible consequence of increasing numbers of axons innervating each mouse soma is that more axons that innervate one soma might also innervate an adjacent soma (i.e., adjacent mouse excitatory neurons "share" more innervation by cohorts of individual inhibitory axons), consistent with previous reports that inhibitory innervation is broad and non-specific (Fino et al., 2013; Packer and Yuste, 2011). We tested this hypothesis by tracing every axon innervating the somata of nearest neighbor excitatory neurons in both species and asked how often these neighboring neurons share inhibitory innervation from the same axon fragment. Figure 4A shows one representative reconstruction from each species from this experiment, and Figure 4B shows quantification of this analysis across three pairs of neurons for each species (i.e., six total neurons/species with pairs of neurons within 15 µm had all their somatic innervating axons

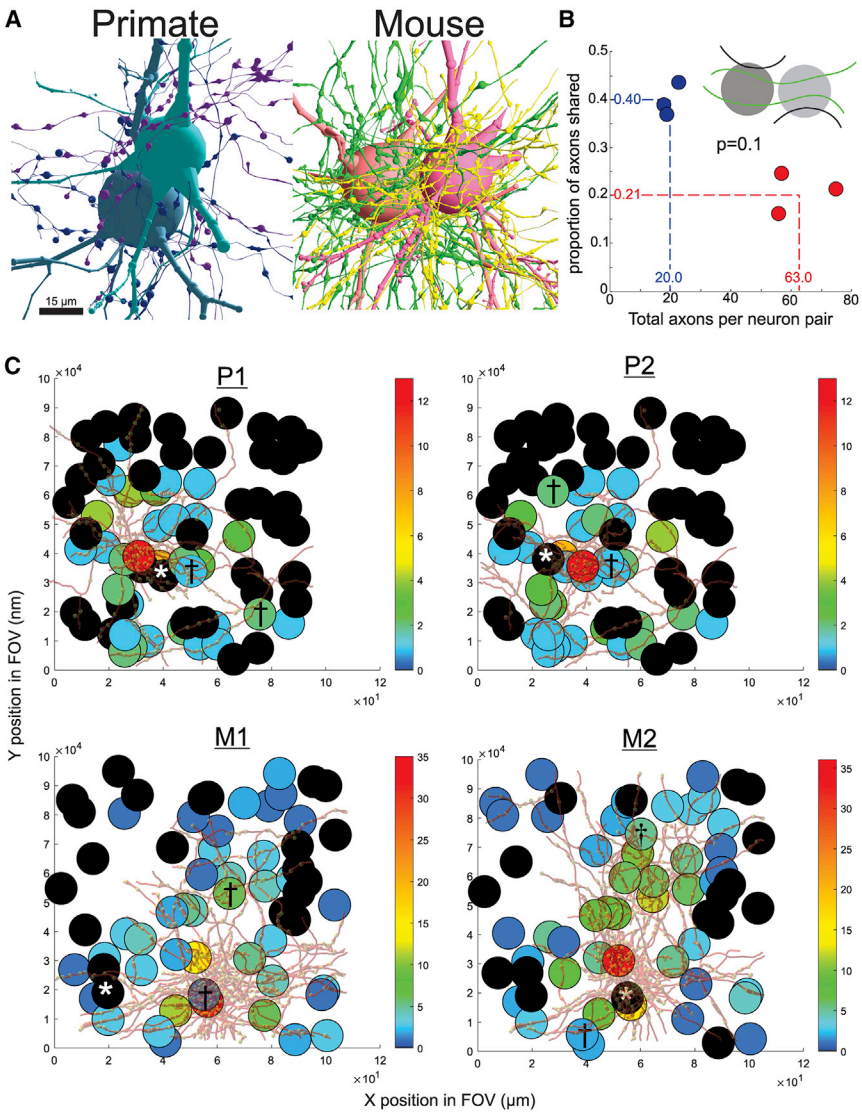

Figure 4. Neighboring primate and mouse excitatory neurons have similar inhibitory networks

(A) Reconstructions of every inhibitory axon innervating the soma of two adjacent L2/3 excitatory neurons (primate: 19 axons, 40 synapses; mouse: 57 axons, 151 synapses).

(B) Inset: shared (green lines) and unshared axons (black lines) between neighboring neuron pairs. Scatterplot of the number of axons synapsed with the soma and perisoma of neighboring neuron pairs versus the proportion of those axons shared between the two neurons (primate: 0.40 ± 0.02 shared axons, n = 60 axons making 162 synapses across three neuron pairs; mouse: 0.21 ± 0.02 shared axons, n = 188 axons making 504 synapses across three neuron pairs; p = 0.1).

(C) Scatterplot of the number of shared axons between a source neuron (red circle) and all neighboring neurons (all other circles). Circle color represents the number of shared axons a given neuron has with the source neuron (see heatmap). Each neuron is plotted in their actual x and y positions with somatic innervating axons (red lines) traced from the source soma overlaid and yellow nodes depict synapses. Asterisks mark examples of nearby neurons that do not share axons with the source neuron. Daggers mark examples of neurons whose number of shared axons with the source neuron do not correlate with distance from the source neuron. Two analyses were performed for each species (primate: P1, n = 10 axons, 145 synapses, 36 neurons; P2, n = 9 axons, 103 synapses, 36 neurons; mouse: M1, n = 32 axons, 455 synapses, 49 neurons; M2, n = 25 axons, 397 synapses, 49 neurons).

All quantifications represent mean ± SEM; p values were calculated using a two-tailed Mann Whitney U test with a 0.05 significance level.

traced). Surprisingly, we found that despite the large difference in absolute numbers of axons that innervated soma across species (i.e., 2.7-fold more axons per soma in the mouse; refer to Figure S6D), in this limited sample size, we observe that primate excitatory neurons were more likely to share inhibitory axonal inputs than mouse neurons (primate, 24 of 60 average axons shared [40%] across three neuronal pairs; mouse, 39 of 188 average axons shared [21%] across three neuronal pairs), but this sample size is likely too small for an accurate estimate of statistical significance (Figure 4B).

Another possibility is that although sharing of presynaptic inhibitory axons is similar across species at short distance (e.g., immediately proximate excitatory neuronal soma), as the distance between excitatory soma increases, more mouse inhibitory inputs are shared than in the primate. Thus, we asked how often axons innervating a particular soma also synapse with the other excitatory neurons throughout the volume. For each species, we traced all inhibitory axons innervating the soma of two excitatory neurons (i.e., "source neuron"; Figure 4C, red circles and corresponding axonal trajectories overlaid, two neurons for each species; primate, P1 and P2; mouse, M1 and M2) and identified every additional synapse these axons made with every other neuron in the volume, establishing the number of shared inhibitory inputs for each neuron in the volume relative to the source neuron (Figure 4C, colored circles). The pattern of inhibitory innervation in both species showed a trend toward both specificity and sparsity of innervation. Neurons separated by 70 μm or greater from the source neuron shared few if any inhibitory axons (i.e., sparsity). Neurons proximate to the source neuron did not always get co-innervated, and locally, distance could not predict the amount of co-innervation (i.e., specificity) (Figure 4C, see soma marked with asterisks and daggers, respectively, for examples). Thus, changes in the absolute numbers of inhibitory inputs on individual neurons across species seems to have little correlation with how inhibitory, presumably PV+, networks connect with excitatory neurons.

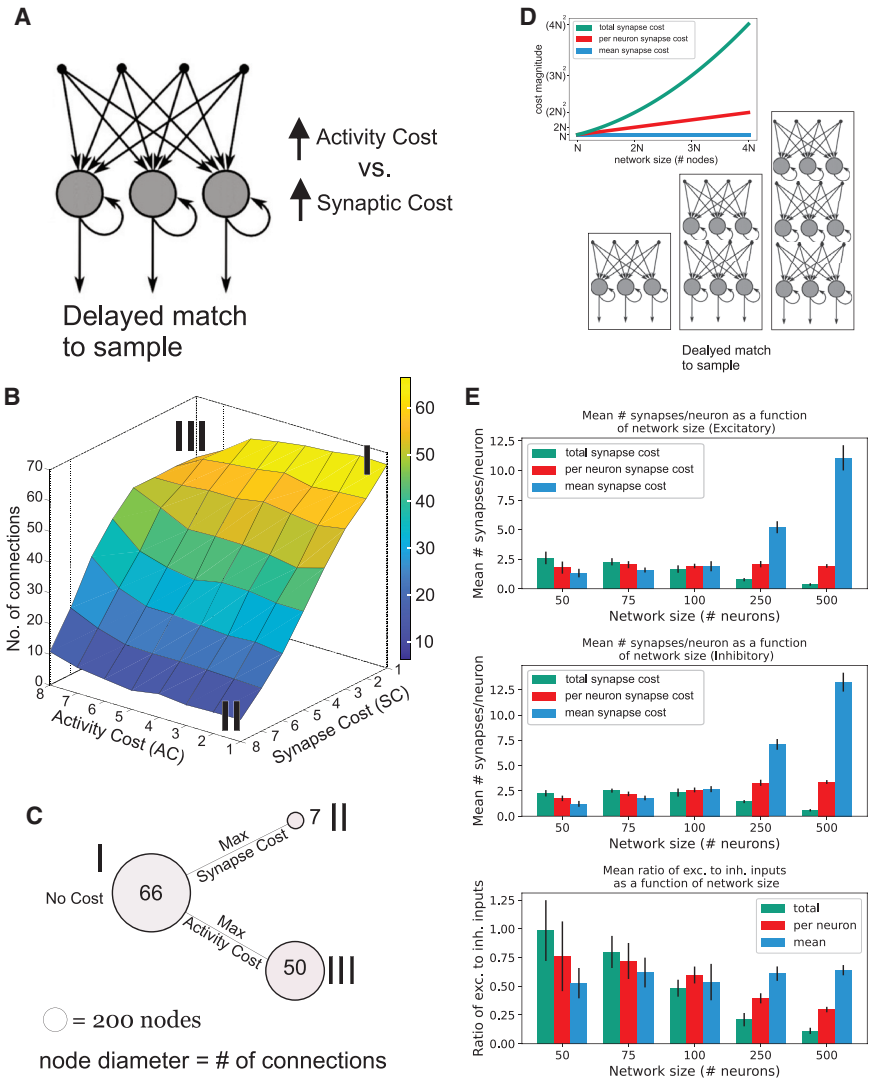

Figure 5. Metabolic costs on firing rates and synaptic machinery regulate connection density in artificial recurrent neural networks

(A) Schematic of the recurrent neural network (RNN). A matrix of RNNs consisting of 200 nodes was constructed, with each RNN having different activity and synapse cost imposed while trained to perform a delayed match-to-sample cognitive task.

(B) Three-dimensional heatmap of connection density of RNNs trained to perform a cognitive task under different costs. For each combination of activity cost (AC) weighting (penalty on mean firing rate) and synapse cost (SC) weighting (penalty on mean connection strength), ten networks were trained to perform the same delayed match-to-sample task. Roman numerals mark extreme points in the matrix: (I) no AC and SC cost; (II) maximum SC, no AC cost; and (III) maximum AC, no SC cost.

(C) Cartoon summarizing RNN results when AC or SC is maximally applied alone. Each circle represents the 200 nodes used for the initial cognitive task in (A), and the size of the circle represents the final number of synapses the network has at the end of the training. With no cost (I; neither SC nor AC) the network has a mean 66 synapses. With a maximum SC cost and no AC cost (II), the network has a mean 7 synapses. With a maximum AC cost and no SC cost (III), the network has a mean 50 synapses.

(D) Inset: line graph of cost magnitude versus network size. Different models of tabulating cost scale differently as network size increases: total synapse cost scales quadratically, synapse cost per neuron scales linearly, and mean synapse cost does not scale. Cartoon: RNNs with different numbers of nodes with a fixed activity cost were trained to perform a delayed match-to-sample cognitive task.

(E) Top/middle: mean number of synapses per neuron (± SD) as a function of network size, shown separately for excitatory neurons (top) and inhibitory neurons (middle). Bottom: mean ratio of excitatory to inhibitory inputs per neuron as a function of network size (± SD). In all cases, n = 10 networks per comparison.

Energy constraints and scaling artificial neural networks

Finally, we hypothesized that the main factor driving the observed differences in neuronal connectivity between mouse and primate was the metabolic cost of maintaining synapses as the number of neurons increases with brain size. To test this idea, we trained recurrent neural networks (RNNs) with separate E/I units performing a cognitive task commonly used in both mouse and macaque studies: delayed match-to-sample task (Dudchenko, 2004; Masse et al., 2018; Yang et al., 2019; Zhang et al., 2019) (Figure 5A; see STAR Methods). We hypothesized that metabolic costs would provide strong evolutionary pressure (Bullmore and Sporns, 2012) for the sparser connectivity we observed in primate neurons, particularly as the number of neurons in primate brains is estimated to be 90 times more than mouse (~6.4 billion in *Macaca mulatta*, ~71 million in *Mus musculus*) (Herculano-Houzel et al., 2006, 2007, 2015). We focused on two forms of "cost": one related to somatic firing rates (activity cost [AC]) and one to building and maintaining synapses (synapse cost [SC]). Importantly, whereas AC was activity dependent, SC was not (i.e., the proliferation of synapses was independent of their activity or AC; see STAR Methods).

We performed two sets of experiments. First, we trained RNNs of fixed numbers of nodes with a range of different AC/SC cost combinations (n = 10 networks per AC/SC combination, 200 nodes) and measured the average numbers of connections per node at the end of training. We find that although increasing AC and SC reduces the number of connections per node after training, the effects of SC on synapse number were far more pronounced than AC (Figures 5B, 5C, and S7A; mean/SD for each

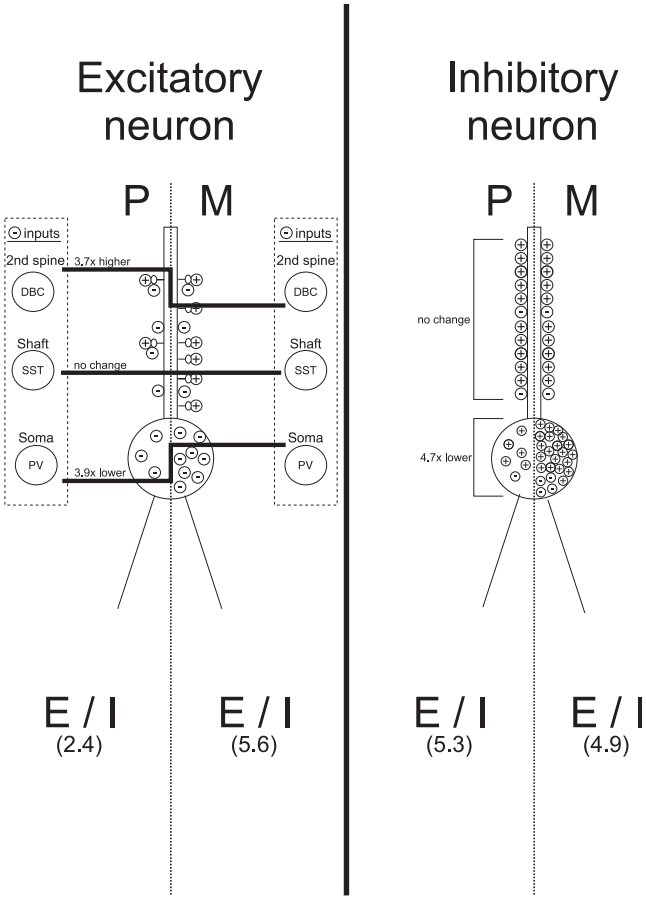

Figure 6. Model of the prototypical primate (P) and mouse (M) L2/3 excitatory and inhibitory neuron

Excitatory neuron: along their dendrites, primate excitatory neurons have fewer excitatory inputs than mouse but equivalent number of shaft inhibitory inputs. Primate neurons have fewer inhibitory inputs onto their somata relative to mouse. Primate excitatory neurons receive 3.7 times higher innervation from dendritic spine innervating inhibitory neurons ("2nd spine synapses"), presumably double bouquet cells (DBC), equivalent dendritic shaft innervation from somatostatin (SST) neurons, and 3.8 times lower somatic innervation by PV+ inhibitory neurons than mouse excitatory neurons. Primate excitatory neurons have a lower E/I ratio (2.4) than mouse (5.6). Inhibitory neuron: along their dendrite, primate inhibitory neurons receive similar synapses/μm but 4.7 times fewer somatic synapses. The E/I ratio is unchanged between primate and mouse inhibitory neurons.

combination reported in the figure). An index of dispersion (IoD) analysis of the mean synapse count per neuron confirmed this conclusion (see STAR Methods). When SC magnitude is fixed and AC magnitude varies, IoDs of mean synapse count are significantly lower than the converse, fixed AC and varied SC (Figure S7B). Analysis of networks with large ACs revealed that activity is minimized predominantly through increases in the numbers of inhibitory connections, unlike the sparsity of inhibitory connections found in the non-human primate brain (Figures S7C and S7D).

We thus focused on the effects of SC as the size of networks increases. We experimented with three models of tabulating the "cost" of synapses in networks of increasing size: (1) total SC, which scales quadratically with the number of nodes; (2) SC per neuron, which scales linearly with the number of neurons; and (3) mean SC, used in experiments described above (Figures 5A–5C), which does not scale with network size (Figure 5D). As networks increase in node size (from 50 to 500 neurons), total synapse penalty produced networks with reductions in excitatory and inhibitory connections and E/I ratio, as seen in the primate EM data (Figure 5E, green bars; least squares fit: slope = −0.009, intercept = 5.11, R^2 = 0.844, p = 5.52e-21, Wald test). Networks penalized instead on synapse number per neuron or mean synapse strength either held constant the number of E synapses and increased the number of I synapses or actually increased the numbers of both E and I connections (Figure 5E; mean strength penalty [blue bars]: least squares fit: slope = 0.049, intercept = −0.129, R^2 = 0.984, p = 6.20e-45, Wald test; synapse strength per neuron penalty [red bars]: least squares fit: slope = 0.003, intercept = 3.958, R^2 = 0.42,p = 3.61e-07, Wald test).

Finally, we performed additional analyses on (1) identical networks (i.e., from Figure 5A) trained on two other benchmark cognitive tasks (Figure S8) (Desimone, 1996; Freedman and Assad, 2006) and (2) different RNNs with costs on synaptic dynamics rather than performance-driven costs, trained on all three cognitive tasks (Figure S9; see STAR Methods) (Masse et al., 2019; Mongillo et al., 2008; Zucker and Regehr, 2002). Across all conditions tested, RNNs converge on the same conclusion: prohibitive energy constraints of building and maintaining synaptic connections drive neural networks of increasing number to be increasingly sparse, as observed in primates versus mouse neurons.

DISCUSSION

Our results directly demonstrate, for the first time, that excitatory primate neurons in L2/3 receive far fewer dendritic inputs (2.4-fold fewer spine synapses), and both excitatory and inhibitory primate neurons receive fewer somatic synapses (4.1-fold) than their mouse counterparts (Figure 6; Table 1), with little change in synapse size. We report large-scale analyses classifying and comparing the ratio of excitatory and inhibitory synapses onto the dendrites and soma of inhibitory neurons across species (Figures 2D and 2E) and differences in the inhibitory innervation patterns on individual spines (i.e., primate spines are ~3.5 times more likely to receive a second synapse). Furthermore, as a result of our reconstructions of axonal wiring, we conclude that basic properties of neuronal networks showed complicated relationships across species: (1) despite receiving fewer total inhibitory inputs onto individual excitatory soma in primates, the proportion of inhibitory axons that connect across excitatory neurons was unchanged between primate and mouse (Figure 4), and (2) primate excitatory neurons showed a lower E/I ratio than equivalent mouse neurons (Figure 1F), but the E/I ratio in mouse and primate inhibitory neurons was unchanged (Figure 2E). Finally, we show, using neurobiologically inspired artificial neural networks trained on multiple cognitive tasks, that as the numbers of nodes (neurons) in networks increase, the number of edges (connections) per node reduces, in line with observations in mouse versus primate neurons. We demonstrate that

the energy costs of creating and maintaining more connections can drive that sparsity *in silico*.

Limitations of study

Here we address potential limitations to the present study. First, our results are gleaned from a limited number of samples: from three mice and two non-human primates and from reconstructions of proximal dendrites <200 um from the soma. These factors could (1) limit the generalizability of these results (e.g., sparsity could be particular to proximal dendrites of primate L2/3 neurons in V1) and (2) leave the potential for confounds from inter-neuronal or inter-individual variances or even differences in synapse density along the dendritic tree (Ballesteros-Yáñez et al., 2006; Bannister and Larkman, 1995; Medalla and Luebke, 2015). This concern is mitigated by several factors. First, we examined the connectivity profiles of many neurons (n > 53; more than 53, because of our random dendrite sampling) and annotated many synapses (n = 15,748) across multiple individuals, and the changes we found in synapse densities and distributions were large and remarkably consistent across neurons in the same species and clearly different across species (Figures 1B–1F; Figures 2B–2E; Table 1). Second, we found similar synapse sparsity in a total of ~2 mm of randomly sampled dendrites of different orientations and diameters in the same volume (Figure 3B), and some of these randomly sample dendrites are likely from different parts of dendritic arbors (e.g., distal versus proximal, main versus side branches, and from somata outside of L2/3). Finally, we found sparse synaptic innervation, both dendritic and somatic, in other primate cortical regions (S1 and LIP) similar to what we observed in V1 (Figures 3D–3F). Moreover, other spine density measurements performed in mouse layer 4 somatosensory cortex (~1.0 spine synapses/μm) (Motta et al., 2019) and layer 3 temporal cortex (1.1 spine synapses/μm) (Benavides-Piccione et al., 2002) agree with our results in mouse L2/3 V1. Thus, we conclude that primate neurons generally receive sparse synapses across multiple cell types and many cortical regions relative to the mouse.

The third limitation is the definition of "adult." With little literature about developmental staging of neuronal connections across species, we chose standard definitions, beyond known critical periods and prior to age-related cognitive decline, and sampled individuals of different ages (mouse: male, 15 weeks old; male, 36 weeks old; and adult mouse, gender and age unreported; primate, 11.0 and 14.5 years old, male). Indeed, future experiments detailing connectivity in developing, "adult," and aged animals will help better establish timelines for comparing connectivity across these and other species.

Finally, there are potential limitations with the volumes analyzed. For example, although we exhaustively traced inhibitory axons within the volume, we cannot exclude the possibility that such axons branched outside of the volume, and thus some of the axonal branches we labeled as independent are the same axon. We believe this limitation is mitigated for several reasons: (1) inspection of individual fluorescently labeled PV+ positive (PV+) soma targeting neurons over larger volumes in mice suggests that although branching is extensive, large branches returning to the same locations are rare (Oliva et al., 2000; Packer et al., 2013), consistent with models of an economy of neuronal wiring (i.e., neuronal wiring minimizes neurite length) (Chklovskii et al., 2002; Karbowski, 2001; Wang and Clandinin, 2016); (2) similar analyses in cortical excitatory neurons suggested that axons rarely branch distally and reinnervate the same target (Kasthuri et al., 2015); and (3) we see no such behavior of inhibitory axons in our volume (all of the branching we observed had no sign of recurrent innervation from distal branches).

Comparison with previous work

Comparisons of how mouse and non-human primate brains differ and are similar have a long history in neuroscience, ranging from how neurons in similar brain regions respond to similar stimuli (Huberman and Niell, 2011; Sanzeni and Histed, 2020; Segev, 1992; Sweeney and Clopath, 2020; Van Hooser, 2007; Wang et al., 2016) to differences in the sizes of brain regions (Van Essen et al., 2018). The prior work perhaps most relevant is generally of two varieties: measurements of bulk synaptic density in neuropil (i.e., synapses/mm^3) in smaller volumes using EM (Ascoli et al., 2008; DeFelipe et al., 1999, 2002; Hsu et al., 2017; McGuire et al., 1991; Medalla and Luebke, 2015; Peters et al., 2008; Sherwood et al., 2020) and optical methods, particularly in primates, whereby neurons in living slices are filled and spines are counted as proxies of excitatory innervation (Gilman et al., 2017; Luebke et al., 2004; Luebke and Rosene, 2003; McGuire et al., 1991; Medalla and Luebke, 2015). The results presented here extend these previous studies and address inherent limitations as described below.

Bulk synapse measurements typically rely on single two-dimensional (2D) EM sections or a small EM series (~50 sections), rarely capturing the full subcellular complement of a neuron. As a result of these smaller volumes, these approaches have several limitations: (1) the layer of origin of parent somata is often unknown, (2) synaptic location on the neuron is often unknown, (3) total synapse numbers for soma are often unknown, and (4) axonal connectivity is often unknown.

Most optical reconstructions of connectivity, particularly in primates, are limited to filling individual neurons with opaque dyes either indirectly (e.g., Golgi staining) or directly, often via injection into living neurons in brain slices and sometimes after electrophysiological characterization (Elston et al., 2011; Gilman et al., 2017). Such reconstructions sample more animals and capture larger fractions of dendritic arbors but suffer potential disadvantages, including (1) incomplete fills of neurons and the use of diffraction-limited optics in dense neuropil frequently results in errors when assigning connectivity (Briggman et al., 2011; Mishchenko et al., 2010), and (2) optical microscopy has little to say about the innervation patterns of synapses on neuronal soma, on dendritic shafts of excitatory neurons, on the dendrites of inhibitory neurons, second spine innervation, or patterns of how putative inhibitory axons innervate excitatory neurons, all novel results presented here for mice and primates.

Last, the majority of spine counting in primate neurons has been accompanied by prior electrophysiological characterization of neurons (Gilman et al., 2017; Luebke et al., 2004; Luebke and Rosene, 2003; Medalla and Luebke, 2015). However, the preparation of living brain slices can induce new spine formation, often twice the number relative to perfusion controls (Kirov et al.,

1999, 2004; Trivino-Paredes et al., 2019). These potential artifacts are particularly problematic in living brain slices chilled prior to recordings, a protocol used for most structural synaptic analyses of primates (Gilman et al., 2017; Luebke et al., 2004; Medalla and Luebke, 2015). As similar studies on the effects of brain slice preparation on spine density have not been done in non-human primates, they offer potential confounds in comparisons of spine densities across species.

Redistributions of synapses on excitatory neurons

A key advantage to connectomic analysis at the scale of neurons is the ability to capture all connections on that neuron within the field of view, as opposed to methods that rely on selectively labeling a subset of connections. In doing so, we find changes in the relative distribution of the types of inhibitory synapses onto primate excitatory neurons relative to mouse: (1) a 4-fold reduction in somatic synapses, without reduction in the size of boutons; (2) an unchanged frequency of dendritic shaft synapses; and (3) a 3-fold increase in the proportion of "second spine" synapses. Collectively, this reduces the potential role of somatic inhibition and increased role for dendritic inhibition on primate neurons. Moreover, with fewer excitatory spine synapses, primate neurons have a lower E/I ratio than mouse neurons (Figure 1F; Table 1), emphasizing the shift toward significantly more inhibition onto primate excitatory neurons. Interestingly, inhibitory neurons that synapse onto excitatory neurons can be broadly classified by where on the postsynaptic excitatory neuron they synapse (e.g., shaft, spine, soma), and moreover, each class of inhibitory neuron is reported to have specific roles in shaping functional responses of excitatory neurons to external stimuli (Kawaguchi and Kubota, 1997; Kepecs and Fishell, 2014; Somogyi et al., 1983; Tremblay et al., 2016). Specifically, PV+ basket cells form the majority of somatic and perisomatic synapses, and somatostatin (SST+) interneurons preferentially target dendritic shafts of excitatory neurons. Reduced somatic and increased dendritic inhibition might support species-specific dendritic processing, as recently reported in human neurons (Gidon et al., 2020). Less is known about specific inhibitory neuronal types preferentially innervating "second synapses" on spines, but in humans and non-human primates, PV−/calbindin+ double bouquet cells (DBCs) seem to fit this bill (Tamás et al., 1997). DBCs are noteworthy because it is unclear whether they exist in rodents (Scala et al., 2019; Yáñez et al., 2005). Thus, species differences in the redistribution of inhibitory synapses could result from changes in the proportions of inhibitory cell types or the presence of novel inhibitory cell types (Džaja et al., 2014; Hodge et al., 2019; Krienen et al., 2020; Sultan and Shi, 2018).

Sparse inhibitory innervation

A fundamental and recurring question in neuroscience is the specificity with which inhibitory neurons target excitatory neuronal populations, and a current hypothesis is that inhibitory connectivity to excitatory neurons is dense and non-specific (Fino et al., 2013; Packer and Yuste, 2011). We address this question with the first exhaustive reconstruction of innervation patterns of somatic targeting inhibitory axons across species, asking how often the complete set of inhibitory axons innervating a given excitatory soma innervate neighboring soma (i.e., are inhibitory connections dense and non-specific?). We find that interneuron connectivity between neurons was sparse: neurons only tens of microns apart were unlikely to "share" the same presynaptic inhibitory axon (Figure 4C). Indeed, we found many instances in which inhibitory axons that synapse on a given soma directly contact other neuronal soma and dendrites without innervating those neurons (data not shown). Interestingly, this aspect of somatic innervation was true across mice and primates despite mouse excitatory neurons receiving ~4-fold more somatic inhibitory synapses, favoring models in which interneurons consistently connect with precision and selectivity (Yoshimura and Callaway, 2005). Finally, we find little change in inhibitory synapse size across species as potential compensation for the reduced number of synapses on primate neurons (Figure S6E) (Arellano et al., 2007; Holler et al., 2021; Holtmaat and Svoboda, 2009).

Energy constraints and scaling natural and *in silico* neural networks

There are broadly two types of models of how brains consume energy relevant to this work. First are models on energy consumption at the level of whole brains, which suggest that as brains grow in the number of neurons, animals consume correspondingly more calories, such that the amount of glucose (or oxygen) used per neuron remains relatively constant (Herculano-Houzel, 2011). Second are models of energy consumption at the level of individual neurons, which suggest that most energy is "spent" primarily on synaptic transmission, with the implication that energy demands of individual neurons scale with its number or size of connections (Attwell and Laughlin, 2001; Harris and Weinberg, 2012). A critical gap is data on how energy demands could potentially constrain connections on individual neurons as brains increase the numbers of neurons. Our simulations suggest that it is the energy cost of creating and maintaining synapses, as opposed to the "costs" of spiking, that drives the sparsity of connections with increased neuronal number across mouse and primate.

STAR★METHODS

Detailed methods are provided in the online version of this paper and include the following:

- KEY RESOURCES TABLE
- RESOURCE AVAILABILITY
  - Lead contact
  - Materials availability
  - Data and code availability
- EXPERIMENTAL MODEL AND SUBJECT DETAILS
- METHOD DETAILS
  - Data acquisition
  - Data analysis
  - Spine and shaft synapse frequency
  - Soma synapses
  - E/I ratio for excitatory neurons
  - E/I ratio for inhibitory neurons
  - Randomly sampled dendrites
  - Inhibitory axons length/branches

SUPPLEMENTAL INFORMATION

Supplemental information can be found online at https://doi.org/10.1016/j.celrep.2021.109709.

ACKNOWLEDGMENTS

We thank J.H.R. Maunsell, S.M. Sherman, V. Jain, B. Dorian, and V. Sampathkumar for discussions; J.H.R. Maunsell and V. Jain for valuable comments on the manuscript; Marek Niekrasz and the entire ARC team for assistance with animal care; H. Li and K. Norwood for computer infrastructure and coding; and Tom Uram at Argonne National Laboratory for assistance with implementing alignment code on Argonne's supercomputer. N.K. was supported by a technical award from the McKnight Foundation, a Brain Initiative NIH grant (U01 MH109100), and a National Science Foundation (NSF) NeuroNex grant.

AUTHOR CONTRIBUTIONS

N.K. and G.A.W. conceived of the experiment and performed analyses. G.A.W. collected the data (sample preparation, imaging, image alignment, and analyses). N.K. and G.A.W. wrote the manuscript. D.P. plotted Figures S1D–S1F. M.R. and J.L. performed all *in silico* RNN experiments (Figures 5 and S7–S10).

DECLARATION OF INTERESTS

The authors declare no competing interests.

Received: June 14, 2021
Revised: July 30, 2021
Accepted: August 20, 2021
Published: September 14, 2021

REFERENCES

Arellano, J.I., Benavides-Piccione, R., Defelipe, J., and Yuste, R. (2007). Ultrastructure of dendritic spines: correlation between synaptic and spine morphologies. Front. Neurosci. *1*, 131–143.

Ascoli, G.A., Alonso-Nanclares, L., Anderson, S.A., Barrionuevo, G., Benavides-Piccione, R., Burkhalter, A., Buzsáki, G., Cauli, B., Defelipe, J., Fairén, A., et al.; Petilla Interneuron Nomenclature Group (2008). Petilla terminology: nomenclature of features of GABAergic interneurons of the cerebral cortex. Nat. Rev. Neurosci. *9*, 557–568.

Attwell, D., and Laughlin, S. (2001). An energy budget for signaling in the grey matter of the brain. J. Cereb. Blood Flow Metab. *10*, 1133–1145. https://doi.org/10.1097/00004647-200110000-00001.

Baena, V., Schalek, R.L., Lichtman, J.W., and Terasaki, M. (2019). Serial-section electron microscopy using automated tape-collecting ultramicrotome (ATUM). Methods Cell Biol. *152*, 41–67.

Bakken, T.E., Miller, J.A., Ding, S.L., Sunkin, S.M., Smith, K.A., Ng, L., Szafer, A., Dalley, R.A., Royall, J.J., Lemon, T., et al. (2016). A comprehensive transcriptional map of primate brain development. Nature *535*, 367–375.

Bakken, T.E., Jorstad, N.L., Hu, Q., and Lein, E.S. (2020). Evolution of cellular diversity in primary motor cortex of human, marmoset monkey, and mouse. bioRxiv. https://doi.org/10.1101/2020.03.31.016972.

Ballesteros-Yáñez, I., Benavides-Piccione, R., Elston, G.N., Yuste, R., and DeFelipe, J. (2006). Density and morphology of dendritic spines in mouse neocortex. Neuroscience *138*, 403–409.

Bannister, N.J., and Larkman, A.U. (1995). Dendritic morphology of CA1 pyramidal neurones from the rat hippocampus: II. Spine distributions. J. Comp. Neurol. *360*, 161–171.

Benavides-Piccione, R., Ballesteros-Yáñez, I., DeFelipe, J., and Yuste, R. (2002). Cortical area and species differences in dendritic spine morphology. J. Neurocytol. *31*, 337–346.

Benavides-Piccione, R., Fernaud-Espinosa, I., Robles, V., Yuste, R., and DeFelipe, J. (2013). Age-based comparison of human dendritic spine structure using complete three-dimensional reconstructions. Cereb. Cortex *23*, 1798–1810.

Bernard, A., Lubbers, L.S., Tanis, K.Q., Luo, R., Podtelezhnikov, A.A., Finney, E.M., McWhorter, M.M., Serikawa, K., Lemon, T., Morgan, R., et al. (2012). Transcriptional architecture of the primate neocortex. Neuron *73*, 1083–1099.

Bock, D.D., Lee, W.C., Kerlin, A.M., Andermann, M.L., Hood, G., Wetzel, A.W., Yurgenson, S., Soucy, E.R., Kim, H.S., and Reid, R.C. (2011). Network anatomy and in vivo physiology of visual cortical neurons. Nature *471*, 177–182.

Bourgeois, J.P., and Rakic, P. (1993). Changes of synaptic density in the primary visual cortex of the macaque monkey from fetal to adult stage. J. Neurosci. *13*, 2801–2820.

Briggman, K.L., Helmstaedter, M., and Denk, W. (2011). Wiring specificity in the direction-selectivity circuit of the retina. Nature *471*, 183–188.

Brunel, N. (2000). Dynamics of sparsely connected networks of excitatory and inhibitory spiking neurons. J. Comput. Neurosci. *8*, 183–208.

Bullmore, E., and Sporns, O. (2012). The economy of brain network organization. Nat. Rev. Neurosci. *13*, 336–349.

Chklovskii, D.B., Schikorski, T., and Stevens, C.F. (2002). Wiring optimization in cortical circuits. Neuron *34*, 341–347.

DeFelipe, J., Marco, P., Busturia, I., and Merchán-Pérez, A. (1999). Estimation of the number of synapses in the cerebral cortex: methodological considerations. Cereb. Cortex *9*, 722–732.

DeFelipe, J., Alonso-Nanclares, L., and Arellano, J.I. (2002). Microstructure of the neocortex: comparative aspects. J. Neurocytol. *31*, 299–316.

Desimone, R. (1996). Neural mechanisms for visual memory and their role in attention. Proc. Natl. Acad. Sci. U S A *93*, 13494–13499.

Dudchenko, P.A. (2004). An overview of the tasks used to test working memory in rodents. Neurosci. Biobehav. Rev. *28*, 699–709.

Džaja, D., Hladnik, A., Bičanić, I., Baković, M., and Petanjek, Z. (2014). Neocortical calretinin neurons in primates: increase in proportion and microcircuitry structure. Front. Neuroanat. *8*, 103.

Elston, G.N., Benavides-Piccione, R., Elston, A., Manger, P.R., and Defelipe, J. (2011). Pyramidal cells in prefrontal cortex of primates: marked differences in neuronal structure among species. Front. Neuroanat. *5*, 2.

Emoto, K., Wong, R., Huang, E., and Hoogenraad, C. (2016). Dendrites: Development and Disease (Springer).

Fino, E., Packer, A.M., and Yuste, R. (2013). The logic of inhibitory connectivity in the neocortex. Neuroscientist *19*, 228–237.

Freedman, D.J., and Assad, J.A. (2006). Experience-dependent representation of visual categories in parietal cortex. Nature *443*, 85–88.

Freund, T.F., and Buzsáki, G. (1996). Interneurons of the hippocampus. Hippocampus *6*, 347–470.

Freund, T.F., and Katona, I. (2007). Perisomatic inhibition. Neuron *56*, 33–42.

Gidon, A., Zolnik, T.A., Fidzinski, P., Bolduan, F., Papoutsi, A., Poirazi, P., Holtkamp, M., Vida, I., and Larkum, M.E. (2020). Dendritic action potentials and computation in human layer 2/3 cortical neurons. Science *367*, 83–87.

Gilman, J.P., Medalla, M., and Luebke, J.I. (2017). Area-specific features of pyramidal neurons—a comparative study in mouse and rhesus monkey. Cereb. Cortex *27*, 2078–2094.

Goldberg, J.H., and Yuste, R. (2005). Space matters: local and global dendritic Ca^{2+} compartmentalization in cortical interneurons. Trends Neurosci. *28*, 158–167.

Goldberg, J.H., Tamas, G., Aronov, D., and Yuste, R. (2003). Calcium microdomains in aspiny dendrites. Neuron *40*, 807–821.

Gour, A., Boergens, K.M., Heike, N., Hua, Y., Laserstein, P., Song, K., and Helmstaedter, M. (2021). Postnatal connectomic development of inhibition in mouse barrel cortex. Science *371*, eabb4534.

Gouwens, N.W., Berg, J., Feng, D., Sorensen, S.A., Zeng, H., Hawrylycz, M.J., Koch, C., and Arkhipov, A. (2018). Systematic generation of biophysically detailed models for diverse cortical neuron types. Nat. Commun. *9*, 710.

Gouwens, N.W., Sorensen, S.A., Berg, J., Lee, C., Jarsky, T., Ting, J., Sunkin, S.M., Feng, D., Anastassiou, C.A., Barkan, E., et al. (2019). Classification of electrophysiological and morphological neuron types in the mouse visual cortex. Nat. Neurosci. *22*, 1182–1195.

Gulyás, A.I., Megías, M., Emri, Z., and Freund, T.F. (1999). Total number and ratio of excitatory and inhibitory synapses converging onto single interneurons of different types in the CA1 area of the rat hippocampus. J. Neurosci. *19*, 10082–10097.

Gur, M., and Snodderly, D.M. (2008). Physiological differences between neurons in layer 2 and layer 3 of primary visual cortex (V1) of alert macaque monkeys. J. Physiol. *586*, 2293–2306.

Harris, K.M., and Weinberg, R.J. (2012). Ultrastructure of synapses in the mammalian brain. Cold Spring Harb. Perspect. Biol. *4*, a005587.

Hayworth, K.J., Peale, D., Januszewski, M., Knott, G.W., Lu, Z., Xu, C.S., and Hess, H.F. (2020). Gas cluster ion beam SEM for imaging of large tissue samples with 10 nm isotropic resolution. Nat. Methods *17*, 68–71.

Herculano-Houzel, S. (2009). The human brain in numbers: a linearly scaled-up primate brain. Front. Hum. Neurosci. *3*, 31.

Herculano-Houzel, S. (2011). Not all brains are made the same: new views on brain scaling in evolution. Brain Behav Evol *78*, 22–36.

Herculano-Houzel, S., Mota, B., and Lent, R. (2006). Cellular scaling rules for rodent brains. Proc. Natl. Acad. Sci. U S A *103*, 12138–12143.

Herculano-Houzel, S., Collins, C.E., Wong, P., and Kaas, J.H. (2007). Cellular scaling rules for primate brains. Proc. Natl. Acad. Sci. U S A *104*, 3562–3567.

Herculano-Houzel, S., Catania, K., Manger, P.R., and Kaas, J.H. (2015). Mammalian brains are made of these: a dataset of the numbers and densities of neuronal and nonneuronal cells in the brain of glires, primates, scandentia, eulipotyphlans, afrotherians and artiodactyls, and their relationship with body mass. Brain Behav Evol *86*, 145–163.

Hering, H., and Sheng, M. (2001). Dendritic spines: structure, dynamics and regulation. Nat. Rev. Neurosci. *2*, 880–888.

Hodge, R.D., Bakken, T.E., Miller, J.A., Smith, K.A., Barkan, E.R., Graybuck, L.T., Close, J.L., Long, B., Johansen, N., Penn, O., et al. (2019). Conserved cell types with divergent features in human versus mouse cortex. Nature *573*, 61–68.

Holler, S., Köstinger, G., Martin, K.A.C., Schuhknecht, G.F.P., and Stratford, K.J. (2021). Structure and function of a neocortical synapse. Nature *591*, 111–116.

Holtmaat, A., and Svoboda, K. (2009). Experience-dependent structural synaptic plasticity in the mammalian brain. Nat. Rev. Neurosci. *10*, 647–658.

Horton, J.C., and Hocking, D.R. (1997). Timing of the critical period for plasticity of ocular dominance columns in macaque striate cortex. J. Neurosci. *17*, 3684–3709.

Hsu, A., Luebke, J.I., and Medalla, M. (2017). Comparative ultrastructural features of excitatory synapses in the visual and frontal cortices of the adult mouse and monkey. J. Comp. Neurol. *525*, 2175–2191.

Hua, Y., Laserstein, P., and Helmstaedter, M. (2015). Large-volume en-bloc staining for electron microscopy-based connectomics. Nat. Commun. *6*, 7923.

Huberman, A.D., and Niell, C.M. (2011). What can mice tell us about how vision works? Trends Neurosci. *34*, 464–473.

Huk, A.C., Katz, L.N., and Yates, J.L. (2017). The role of the lateral intraparietal area in (the study of) decision making. Annu. Rev. Neurosci. *40*, 349–372.

Isaacson, J.S., and Scanziani, M. (2011). How inhibition shapes cortical activity. Neuron *72*, 231–243.

Januszewski, M., Kornfeld, J., Li, P.H., Pope, A., Blakely, T., Lindsey, L., Maitin-Shepard, J., Tyka, M., Denk, W., and Jain, V. (2018). High-precision automated reconstruction of neurons with flood-filling networks. Nat. Methods *15*, 605–610.

Jones, E.G., and Powell, T.P. (1969). Morphological variations in the dendritic spines of the neocortex. J. Cell Sci. *5*, 509–529.

Kanari, L., Ramaswamy, S., Shi, Y., Morand, S., Meystre, J., Perin, R., Abdellah, M., Wang, Y., Hess, K., and Markram, H. (2019). Objective morphological classification of neocortical pyramidal cells. Cereb. Cortex *29*, 1719–1735.

Karbowski, J. (2001). Optimal wiring principle and plateaus in the degree of separation for cortical neurons. Phys. Rev. Lett. *86*, 3674–3677.

Karube, F., Kubota, Y., and Kawaguchi, Y. (2004). Axon branching and synaptic bouton phenotypes in GABAergic nonpyramidal cell subtypes. J. Neurosci. *24*, 2853–2865.

Kasthuri, N., Hayworth, K.J., Berger, D.R., Schalek, R.L., Conchello, J.A., Knowles-Barley, S., Lee, D., Vázquez-Reina, A., Kaynig, V., Jones, T.R., et al. (2015). Saturated reconstruction of a volume of neocortex. Cell *162*, 648–661.

Kawaguchi, Y., and Kubota, Y. (1997). GABAergic cell subtypes and their synaptic connections in rat frontal cortex. Cereb. Cortex *7*, 476–486.

Kepecs, A., and Fishell, G. (2014). Interneuron cell types are fit to function. Nature *505*, 318–326.

Kirov, S.A., Sorra, K.E., and Harris, K.M. (1999). Slices have more synapses than perfusion-fixed hippocampus from both young and mature rats. J. Neurosci. *19*, 2876–2886.

Kirov, S.A., Petrak, L.J., Fiala, J.C., and Harris, K.M. (2004). Dendritic spines disappear with chilling but proliferate excessively upon rewarming of mature hippocampus. Neuroscience *127*, 69–80.

Kisvárday, Z.F., Martin, K.A., Whitteridge, D., and Somogyi, P. (1985). Synaptic connections of intracellularly filled clutch cells: a type of small basket cell in the visual cortex of the cat. J. Comp. Neurol. *241*, 111–137.

Knott, G.W., Quairiaux, C., Genoud, C., and Welker, E. (2002). Formation of dendritic spines with GABAergic synapses induced by whisker stimulation in adult mice. Neuron *34*, 265–273.

Kremkow, J., Perrinet, L.U., Masson, G.S., and Aertsen, A. (2010). Functional consequences of correlated excitatory and inhibitory conductances in cortical networks. J. Comput. Neurosci. *28*, 579–594.

Krienen, F.M., Goldman, M., Zhang, Q., C H Del Rosario, R., Florio, M., Machold, R., Saunders, A., Levandowski, K., Zaniewski, H., Schuman, B., et al. (2020). Innovations present in the primate interneuron repertoire. Nature *586*, 262–269.

Kwon, T., Merchán-Pérez, A., Rial Verde, E.M., Rodríguez, J.R., DeFelipe, J., and Yuste, R. (2019). Ultrastructural, molecular and functional mapping of GABAergic synapses on dendritic spines and shafts of neocortical pyramidal neurons. Cereb. Cortex *29*, 2771–2781.

Lee, C.K., Weindruch, R., and Prolla, T.A. (2000). Gene-expression profile of the ageing brain in mice. Nat. Genet. *25*, 294–297.

Lee, W.C., Bonin, V., Reed, M., Graham, B.J., Hood, G., Glattfelder, K., and Reid, R.C. (2016). Anatomy and function of an excitatory network in the visual cortex. Nature *532*, 370–374.

Luebke, J.I., and Rosene, D.L. (2003). Aging alters dendritic morphology, input resistance, and inhibitory signaling in dentate granule cells of the rhesus monkey. J. Comp. Neurol. *460*, 573–584.

Luebke, J.I., Chang, Y.M., Moore, T.L., and Rosene, D.L. (2004). Normal aging results in decreased synaptic excitation and increased synaptic inhibition of layer 2/3 pyramidal cells in the monkey prefrontal cortex. Neuroscience *125*, 277–288.

Marx, A., Backes, C., Meese, E., Lenhof, H.P., and Keller, A. (2016). EDISON-WMW: exact dynamic programing solution of the Wilcoxon-Mann-Whitney test. Genomics Proteomics Bioinformatics *14*, 55–61.

Masse, N.Y., Grant, G.D., and Freedman, D.J. (2018). Alleviating catastrophic forgetting using context-dependent gating and synaptic stabilization. Proc. Natl. Acad. Sci. U S A *115*, E10467–E10475.

Masse, N.Y., Yang, G.R., Song, H.F., Wang, X.J., and Freedman, D.J. (2019). Circuit mechanisms for the maintenance and manipulation of information in working memory. Nat. Neurosci. *22*, 1159–1167.

McGuire, B.A., Gilbert, C.D., Rivlin, P.K., and Wiesel, T.N. (1991). Targets of horizontal connections in macaque primary visual cortex. J. Comp. Neurol. *305*, 370–392.

Medalla, M., and Luebke, J.I. (2015). Diversity of glutamatergic synaptic strength in lateral prefrontal versus primary visual cortices in the rhesus monkey. J. Neurosci. *35*, 112–127.

Megías, M., Emri, Z., Freund, T.F., and Gulyás, A.I. (2001). Total number and distribution of inhibitory and excitatory synapses on hippocampal CA1 pyramidal cells. Neuroscience *102*, 527–540.

Mishchenko, Y., Hu, T., Spacek, J., Mendenhall, J., Harris, K.M., and Chklovskii, D.B. (2010). Ultrastructural analysis of hippocampal neuropil from the connectomics perspective. Neuron *67*, 1009–1020.

Mongillo, G., Barak, O., and Tsodyks, M. (2008). Synaptic theory of working memory. Science *319*, 1543–1546.

Motta, A., Berning, M., Boergens, K.M., Staffler, B., Beining, M., Loomba, S., Hennig, P., Wissler, H., and Helmstaedter, M. (2019). Dense connectomic reconstruction in layer 4 of the somatosensory cortex. Science *366*, eaay3134.

Ohki, K., Chung, S., Ch'ng, Y.H., Kara, P., and Reid, R.C. (2005). Functional imaging with cellular resolution reveals precise micro-architecture in visual cortex. Nature *433*, 597–603.

Oliva, A.A., Jr., Jiang, M., Lam, T., Smith, K.L., and Swann, J.W. (2000). Novel hippocampal interneuronal subtypes identified using transgenic mice that express green fluorescent protein in GABAergic interneurons. J. Neurosci. *20*, 3354–3368.

Packer, A.M., and Yuste, R. (2011). Dense, unspecific connectivity of neocortical parvalbumin-positive interneurons: a canonical microcircuit for inhibition? J. Neurosci. *31*, 13260–13271.

Packer, A.M., McConnell, D.J., Fino, E., and Yuste, R. (2013). Axo-dendritic overlap and laminar projection can explain interneuron connectivity to pyramidal cells. Cereb. Cortex *23*, 2790–2802.

Paxinos, G. (2009). The Rhesus Monkey Brain in Stereotaxic Coordinates, 2nd (Academic).

Peters, A., Rosene, D.L., Moss, M.B., Kemper, T.L., Abraham, C.R., Tigges, J., and Albert, M.S. (1996). Neurobiological bases of age-related cognitive decline in the rhesus monkey. J. Neuropathol. Exp. Neurol. *55*, 861–874.

Peters, A., Sethares, C., and Luebke, J.I. (2008). Synapses are lost during aging in the primate prefrontal cortex. Neuroscience *152*, 970–981.

Radnikow, G., and Feldmeyer, D. (2018). Layer- and Cell Type-Specific Modulation of Excitatory Neuronal Activity in the Neocortex. Front. Neuroanat. *12*, 1.

Rojo, C., Leguey, I., Kastanauskaite, A., Bielza, C., Larrañaga, P., DeFelipe, J., and Benavides-Piccione, R. (2016). Laminar differences in dendritic structure of pyramidal neurons in the juvenile rat somatosensory cortex. Cereb. Cortex *26*, 2811–2822.

Sanzeni, A., and Histed, M.H. (2020). Finding patterns in cortical responses. eLife *9*, e56234.

Scala, F., Kobak, D., Shan, S., Bernaerts, Y., Laturnus, S., Cadwell, C.R., Hartmanis, L., Froudarakis, E., Castro, J.R., Tan, Z.H., et al. (2019). Layer 4 of mouse neocortex differs in cell types and circuit organization between sensory areas. Nat. Commun. *10*, 4174.

Scott, J.A., Grayson, D., Fletcher, E., Lee, A., Bauman, M.D., Schumann, C.M., Buonocore, M.H., and Amaral, D.G. (2016). Longitudinal analysis of the developing rhesus monkey brain using magnetic resonance imaging: birth to adulthood. Brain Struct. Funct. *221*, 2847–2871.

Segev, I. (1992). Single neurone models: oversimple, complex and reduced. Trends Neurosci. *15*, 414–421.

Semple, B.D., Blomgren, K., Gimlin, K., Ferriero, D.M., and Noble-Haeusslein, L.J. (2013). Brain development in rodents and humans: Identifying benchmarks of maturation and vulnerability to injury across species. Prog. Neurobiol. *106–107*, 1–16.

Sherwood, C.C., Miller, S.B., Karl, M., Stimpson, C.D., Phillips, K.A., Jacobs, B., Hof, P.R., Raghanti, M.A., and Smaers, J.B. (2020). Invariant synapse density and neuronal connectivity scaling in primate neocortical evolution. Cereb. Cortex *30*, 5604–5615.

Somogyi, P. (1989). Synaptic organization of GABAergic neurons and $GABA_A$ receptors in the lateral geniculate nucleus and visual cortex. In Neural Mechanisms of Visual Perception, D.K.-T. Lam and C.D. Gilbert, eds. (Portfolio Publishing).

Somogyi, P., Kisvárday, Z.F., Martin, K.A., and Whitteridge, D. (1983). Synaptic connections of morphologically identified and physiologically characterized large basket cells in the striate cortex of cat. Neuroscience *10*, 261–294.

Strata, P., and Harvey, R. (1999). Dale's principle. Brain Res. Bull. *50*, 349–350.

Stuart, G., Spruston, N., and Hausser, M. (2016). Dendrites, 3rd (Oxford University Press).

Sultan, K.T., and Shi, S.H. (2018). Generation of diverse cortical inhibitory interneurons. Wiley Interdiscip. Rev. Dev. Biol. *7*.

Sweeney, Y., and Clopath, C. (2020). Population coupling predicts the plasticity of stimulus responses in cortical circuits. eLife *9*, e56053.

Tamás, G., Buhl, E.H., and Somogyi, P. (1997). Fast IPSPs elicited via multiple synaptic release sites by different types of GABAergic neurone in the cat visual cortex. J. Physiol. *500*, 715–738.

Tasic, B., Menon, V., Nguyen, T.N., Kim, T.K., Jarsky, T., Yao, Z., Levi, B., Gray, L.T., Sorensen, S.A., Dolbeare, T., et al. (2016). Adult mouse cortical cell taxonomy revealed by single cell transcriptomics. Nat. Neurosci. *19*, 335–346.

Tasic, B., Yao, Z., Graybuck, L.T., Smith, K.A., Nguyen, T.N., Bertagnolli, D., Goldy, J., Garren, E., Economo, M.N., Viswanathan, S., et al. (2018). Shared and distinct transcriptomic cell types across neocortical areas. Nature *563*, 72–78.

Tremblay, R., Lee, S., and Rudy, B. (2016). GABAergic interneurons in the neocortex: from cellular properties to circuits. Neuron *91*, 260–292.

Trivino-Paredes, J.S., Nahirney, P.C., Pinar, C., Grandes, P., and Christie, B.R. (2019). Acute slice preparation for electrophysiology increases spine numbers equivalently in the male and female juvenile hippocampus: a DiI labeling study. J. Neurophysiol. *122*, 958–969.

Turner, N.L., Macrina, T., Bae, J.A., Yang, R., Wilson, A.M., Schneider-Mizell, C., Lee, K., Lu, R., Wu, J., Bodor, A.L., et al. (2020). Multiscale and multimodal reconstruction of cortical structure and function. bioRxiv. https://doi.org/10.1101/2020.10.14.338681.

Van Essen, D.C., Donahue, C.J., and Glasser, M.F. (2018). Development and evolution of cerebral and cerebellar cortex. Brain Behav Evol *91*, 158–169.

Van Hooser, S.D. (2007). Similarity and diversity in visual cortex: is there a unifying theory of cortical computation? Neuroscientist *13*, 639–656.

van Vreeswijk, C., and Sompolinsky, H. (1996). Chaos in neuronal networks with balanced excitatory and inhibitory activity. Science *274*, 1724–1726.

Vaudin, M., Wolstenholme, A.J., Tsiquaye, K.N., Zuckerman, A.J., and Harrison, T.J. (1988). The complete nucleotide sequence of the genome of a hepatitis B virus isolated from a naturally infected chimpanzee. J. Gen. Virol. *69*, 1383–1389.

Vishwanathan, A., Ramirez, A., Wu, J., Sood, J., Yang, R., Kemnitz, N., Ih, D., Turner, N., Lee, K., Tartavull, I., et al. (2020). Modularity and neural coding from a brainstem synaptic wiring diagram. bioRxiv. https://doi.org/10.1101/2020.10.28.359620.

Vogels, T.P., and Abbott, L.F. (2009). Gating multiple signals through detailed balance of excitation and inhibition in spiking networks. Nat. Neurosci. *12*, 483–491.

Wang, I.E., and Clandinin, T.R. (2016). The influence of wiring economy on nervous system evolution. Curr. Biol. *26*, R1101–R1108.

Wang, B., Ke, W., Guang, J., Chen, G., Yin, L., Deng, S., He, Q., Liu, Y., He, T., Zheng, R., et al. (2016). Firing frequency maxima of fast-spiking neurons in human, monkey, and mouse neocortex. Front. Cell. Neurosci. *10*, 239.

Wang, Y., Ye, M., Kuang, X., Li, Y., and Hu, S. (2018). A simplified morphological classification scheme for pyramidal cells in six layers of primary somatosensory cortex of juvenile rats. IBRO Rep. *5*, 74–90.

Yáñez, I.B., Muñoz, A., Contreras, J., Gonzalez, J., Rodriguez-Veiga, E., and DeFelipe, J. (2005). Double bouquet cell in the human cerebral cortex and a comparison with other mammals. J. Comp. Neurol. *486*, 344–360.

Yang, G.R., Joglekar, M.R., Song, H.F., Newsome, W.T., and Wang, X.J. (2019). Task representations in neural networks trained to perform many cognitive tasks. Nat. Neurosci. *22*, 297–306.

Yin, W., Brittain, D., Borseth, J., Scott, M.E., Williams, D., Perkins, J., Own, C.S., Murfitt, M., Torres, R.M., Kapner, D., et al. (2020). A petascale automated imaging pipeline for mapping neuronal circuits with high-throughput transmission electron microscopy. Nat. Commun. *11*, 4949.

Yoshimura, Y., and Callaway, E.M. (2005). Fine-scale specificity of cortical networks depends on inhibitory cell type and connectivity. Nat. Neurosci. *8*, 1552–1559.

Zhang, X., Yan, W., Wang, W., Fan, H., Hou, R., Chen, Y., Chen, Z., Ge, C., Duan, S., Compte, A., and Li, C.T. (2019). Active information maintenance in working memory by a sensory cortex. eLife *8*, e43191.

Zucker, R.S., and Regehr, W.G. (2002). Short-term synaptic plasticity. Annu. Rev. Physiol. *64*, 355–405.

STAR★METHODS

KEY RESOURCES TABLE

REAGENT or RESOURCE	SOURCE	IDENTIFIER
Biological samples		
Mouse brain (C57BL/6J) (15 week old mouse)	The Jackson Laboratory	000664
Rhesus Macaque brain (11 and 14.5 year old primate)	David Freedman lab	Provided by collaborators
Deposited data		
Volumetric EM data	Neurodata: https://neurodata.io/	This study
Volumetric EM data neuron morphology annotations	NeuroMorpho.org	Archive Name: Wildenberg
Software and algorithms		
Knossos	Knossos-3D Image Visualization and Annotation	https://knossos.app/
Fiji	ImageJ/Fiji	https://imagej.net/software/fiji/
Aligntk	National Center for Multiscale Modeling of Biological Systems (MMBioS)	https://mmbios.pitt.edu/aligntk-home
MATLAB	MATLAB	https://www.mathworks.com/products/matlab.html
Excel	Microsoft	https://www.microsoft.com/en-us/microsoft-365/excel
Klab utilities for image adjustments/alignment	Github	https://github.com/Hanyu-Li/klab_utils
Custom scripts from processing Knossos nml annotation files	Github	https://github.com/knorwood0/MNRVA

RESOURCE AVAILABILITY

Lead contact

Further information and requests for resources and reagents should be directed to and will be fulfilled by the lead contact, Narayanan Kasthuri (bobbykasthuri@uchicago.edu).

Materials availability

This study did not generate new unique reagents.

Data and code availability

- Data reported in this paper will be shared by the lead contact upon request. Raw EM data and MATLAB code used for data analysis is stored on our local servers and freely available upon request. Additionally, data will be hosted on public databases including https://neurodata.io/ and NeuroMorpho.org. Two additional mouse V1, L2/3 datasets (each ~80 μm x ~80 μm x ~30 μm) were downloaded from previously published articles as tiff stacks from https://neurodata.io/project/ocp/#data using scripts provided by the website. For Bock et al., the pixel coordinates downloaded were: x: 69098-89416, y: 57560-77751, z: 3308-4057 and for Lee et al., x: 69725-90169, y: 81602-102994, z: 1-820. Data was then converted into a Knossos file for reconstructions.
- All original code has been deposited at [repository] and is publicly available as of the date of publication. Github links are listed in the key resources table.
- Any additional information required to reanalyze the data reported in this paper is available from the lead contact upon request.

EXPERIMENTAL MODEL AND SUBJECT DETAILS

1 mouse (male mouse, 15 weeks old, The Jackson Laboratory, #000664) and 2 primates (males, 11 and 14.5 years old; provided by collaborators: Freedman lab (UChicago)) were used in this study. Perfusion procedures were followed according to animal regulations at the University of Chicago's Animal Resources Center (ARC) and approved IACUC protocols. The rhesus macaques and mice were housed in accordance with the *Guide for the Care and Use of Laboratory Animals,* Public Health Service Policy, and the Animal Welfare Act and Regulations, at the University of at Chicago, a fully AAALAC-accredited institution. All procedures involving animal care and use were approved by the IACUC at the University of Chicago.

METHOD DETAILS

Data acquisition

Brains for primate and mouse were prepared as previously described (Hua et al., 2015). For the primate brain, V1 was identified using anatomical landmarks (e.g., calcarine sulcus) and comparing with a published atlas (Paxinos, 2009). Mouse V1 was identified using the Allen Brain Institute reference atlas (http://mouse.brain-map.org/experiment/thumbnails/100048576?image_type=atlas). S1 was identified in the primate brain using the lateral, central and cingulate sulci as areal fiducials and excising a ~1mmx2mm piece of Brodmann's area 3b along the central sulcus. LIP was identified in the primate brain using the intraparietal, lateral, and superior sulcus as areal fiducials and excising a ~1mmx2mm piece of LIP along the intraparietal sulcus (Paxinos, 2009). 3,000, 40nm thick sections were collected and imaged as previously described (Kasthuri et al., 2015).

Data analysis

Data annotations were done by two individuals (GW, BK). To ensure accuracy of the data, ~33% of the annotations from one person was verified by the other. 33% of the annotations were given to a naive annotator to verify the accuracy. We found a > 98% agreement between manual annotators. We found that 100% of spines could be reconstructed. Neurons were reconstructed by first identifying the soma followed by tracing their dendritic arbors. All soma along with their dendrites contained within the volume were reconstructed. Classes of cell types were identified by distinguishing anatomical properties: Excitatory neurons by the presences of dendritic spines, interneurons by the lack of spines and numerous shaft synapses, glial cells by their extensive branching, lack of spines and synapses, and cytoplasmic granules. Skeleton information was exported into tab delimited matrices using homemade Python scripts. Two-tailed Mann Whitney U statistics test with a 0.05 significance level was used (Marx et al., 2016) between aggregate mouse and aggregate primate datasets. Whiskers on boxplots indicate variability outside the upper and lower quartiles and center black line indicates the mean.

Spine and shaft synapse frequency

dendrites of multiple neurons were divided into ~10μm segments that sampled apical and basal dendrites at varying distances from the soma. The number of spine or shaft synapses contained within the 10 μm window were counted manually in Knossos and the total number of synapses were divided by the segment length to calculate spine synapses/μm and shaft synapses/μm. Synapses were identified by the presence of a post-synaptic density and vesicles on the pre-synaptic axon. The distance between the furthest point of the 10μm segment and the soma was computed using the Euclidian distance formula to calculate the distance from the soma.

Soma synapses

excitatory and inhibitory soma were identified as described above. Neurons whose soma was fully within the imaged volume were used to count the total number of soma synapses. Perisomatic synapses were scored along the first 10μm of dendrite that left the soma.

E/I ratio for excitatory neurons

E/I = total spine synapses / (total shaft + total soma/perisoma + total second spine synapses). total spine synapses = spine synapse density * average total dendritic length; Inhibitory: total shaft = shaft synapse density * average total dendritic length; total soma/perisoma = total soma + perisoma synapse number; total 2^{nd} spine synapse = 2^{nd} spines/spine * total spine. Total lengths were derived from published measurements (Gilman et al., 2017).

E/I ratio for inhibitory neurons

number of excitatory synapses divided by inhibitory synapses. Axons were classified as excitatory or inhibitory by the scheme detailed in Figure S4.

Randomly sampled dendrites

a dendrite was chosen at random and traced for 10 μm to first determine if it was an excitatory. Spine synapses were counted within the 10 μm window as described above. The diameter of the dendrite was calculated by measuring across the diameter in all three orthogonal views and then averaged.

Inhibitory axons length/branches

branches were scored manually and length was calculated from Knossos annotations using custom scripts.

Number of soma synapses from inhibitory axons was derived from reconstructions and synapse annotations used for Figure 5.

Bouton size

node radius was used to calculate the surface area using S.A = $\pi 4r^2$

Inhibitory axons across neurons

All somatic synapses were first identified and marked in Knossos between two pairs of neighboring excitatory neurons that were as physically close to each other as possible (~10 μm from center of soma mass), and whose soma are fully contained within the imaged volume. These somatic synapses were used as seed points for fully reconstructing inhibitory axons and every synapse these axons made with both pairs of neurons was annotated for the type of synapse (soma, perisoma, shaft, 2nd spine). The proportion of axons that synapsed with both neighboring neurons was then calculated from the axon reconstructions to determine how many axons were shared between the two neurons. Every soma within the volume had their dendrites first reconstructed. Next, all somatic synapses were identified and marked on a central soma that was fully contained within the volume. These somatic synapses were used as seed points for fully reconstructing inhibitory axons and every synapse these axons made was annotated for the type of synapse (soma, perisoma, shaft, second spine) and which neuron in the FOV it synapsed with. If the postsynaptic target was a dendrite that did not have a reconstruction associated with it (i.e., not associated with a neuron within the volume, the dendrite was followed through the volume to ensure that it left the volume as an orphan dendrite belonging to a neuron outside the imaged volume.

Inter-soma distance

The position of 71 (primate) or 61 (mouse) soma in contained within the high res L2/3 volume was marked in and every pairwise Euclidian distance between the center of mass of every soma was calculated. Results in the low- and high- resolution datasets were the same. Figure S2C shows the low-resolution result. Soma/mm^3 measurements: Across 2 primates and 3 mice, non-overlapping sub-volumes (100 × 100 × 50 μm were sectioned off and all soma wholly contained inside the sub-volume were counted to calculate soma/mm^3.

Branches per neuron

For every neuron in the L2/3 low resolution (40nm) dataset, we reconstructed the length of dendrite contained within the imaged volume from manual reconstructions.

Soma surface area

L2/3 soma in only soma wholly contained within the high resolution L2/3 dataset were used for analysis. Nodes were sized to the approximate size of the soma to determine the pixel diameter which was then converted to soma surface area in μm^2.

Neuron dendrite length

reconstructions of L2/3 neurons from the low resolution (40nm) dataset were used to calculate total dendrite length.

QUANTIFICATION AND STATISTICAL ANALYSIS

Quantification and statistical tests of anatomical measurements

Mean and standard error of the mean (SEM) was calculated for every quantification. Statistical significance was calculated using the two-tailed Mann-Whitney U test with a 0.05 significance level (Marx et al., 2016) between aggregate mouse and aggregate primate datasets. See Table 1 and Figure Legends for the exact value of (n) and what (n) represents.

Artificial recurrent neural networks

Results were also obtained and compared across 3 total tasks and 2 network types. Networks consisted of excitatory and inhibitory units obeying Dale's law (4 excitatory units for each inhibitory unit). Synapses in these networks were also subject to short-term synaptic plasticity according to the method previously described (Masse et al., 2018), with 50% of synapses briefly facilitated by presynaptic activity and 50% briefly depressed. Training occurred through supervised learning; network parameters (weights and biases) were adjusted using the backpropagation-through-time algorithm to minimize the categorical cross-entropy loss $L(\hat{y}, y)$ between predicted output $\hat{y}$ and true output y. Weights were initialized randomly using a gamma distribution and constrained to be strictly positive; as a synapse's weight is pushed below 0 in magnitude during training, it is effectively pruned, ceasing to affect network output and receiving no further adjustment. All networks were trained to stable, comparable levels of performance (> 90% accuracy on the DMS task, Figure S10). After training, synapses were counted as the number of outgoing weights with positive magnitude. Networks were trained in Python using the Tensorflow framework; code implementing this training process, along with all relevant hyperparameters for reproduction, is available on Github.

Metabolic costs

Metabolic costs on neural activity and synapse size were implemented through components added to the cross-entropy loss function used during RNN training. The activity cost (AC) is given by $\frac{1}{t}\lambda_{AC}\sum_{i=0}^{t} h_i$, the mean of all neurons' activity across all time points of a trial. The synapse cost (SC) is given by $\frac{1}{n^2}\lambda_{SC}\sum_{i,j} w_{ij}$, the mean synapse weight between all pairs of a network's n neurons. Two other variants of SC were also used (Figures 6D and 6E): $\frac{1}{n}\lambda_{SC}\sum_{i,j} w_{ij}$, a penalty on the total synapse weight per neuron in a network, and $\lambda_{SC}\sum_{i,j} w_{ij}$, a penalty on the total weight of all synapses in the network. Each of these costs was multiplied by a constant factor, λ, titrating that cost's relative strength during training. Increasing λ_{AC} increased the strength of the activity cost during training, constraining networks more strongly to adopt solutions with lower average activity; similarly, increasing λ_{SC} constrained networks more strongly to adopt solutions with lower synaptic weights. The maximal values of λ_{AC} and λ_{SC} tested and reported here were chosen based on their compatibility with stable network training. After increasing λ_{AC} and λ_{SC} no longer yielded networks that could consistently be trained past 90% accuracy on the DMS task, corresponding with inappropriately strong regularization, λ_{AC} and λ_{SC} were capped, with subsequent analyses restricted to groups of networks with λ_{AC} and λ_{SC} below the threshold of instability.